國 立 交 通 大 學

光電系統研究所

碩士論文

奈米小球填補磷酸與氫氧化鉀之蝕刻缺陷在紫外光發光二極體的應用

Defect Passivation by Nanospheres Using H_3PO_4 and KOH Etching for UV LED

研 究 生 : 馬印聰　　　　指導教授 : 林建中 博士

中華民國一百零一年七月

奈米小球填補磷酸與氫氧化鉀之蝕刻缺陷在紫外光發光二極體的應用

Defect Passivation by Nanospheres Using H_3PO_4 and KOH Etching for UV LED

研 究 生 ： 馬印聰　　Student ： Yin-Tsung Ma

指導教授 ： 林建中　　Advisor ： Chien-Chung Lin

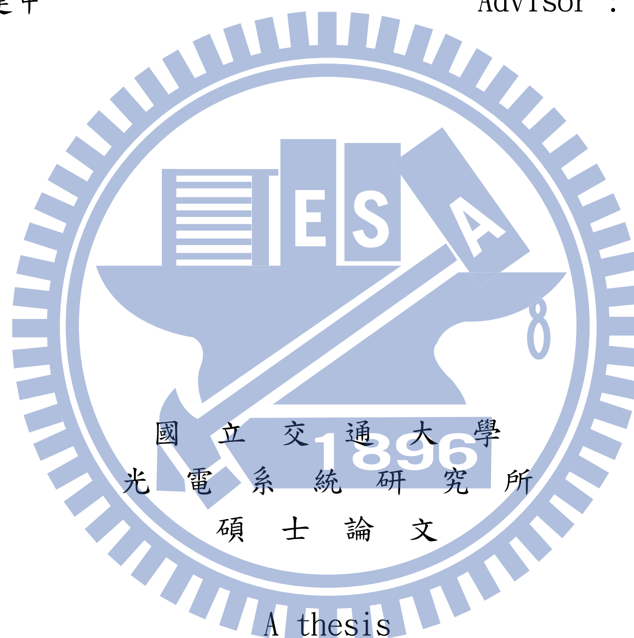

國 立 交 通 大 學

光 電 系 統 研 究 所

碩 士 論 文

A thesis

Submitted to institute of Photonic System

College of Photonics

National Chiao Tung University

In Partial Fulfillment of the Requirements

For the Degree of

Master

In

Photonic System

July 2012

Tainan, Taiwan, Republic of China

中華民國 一百零一 年 七 月

奈米小球填補磷酸與氫氧化鉀之蝕刻缺陷在紫外光發光二極體的應用

研究生 ： 馬印聰　　　　　　　指導教授 ： 林建中 博士

國立交通大學光電系統研究所

中文摘要

本論文中, 我們比較了磷酸與氫氧化鉀蝕刻液在氮化鎵表面上所造成的缺陷型態, 並且發現磷酸所蝕刻出的缺陷型態對應至非輻射複合中心.

我們對此非幅射複合中心做缺陷阻擋, 發現重新成長發光二極體結構後, 其內部量子效應提升了 17.1%.

同時我們使用矽膠奈米小球當作阻擋材料做成發光二極體, 簡化了傳統式電漿增強化學氣相沉積法. 在反射率的表現上, 接近 361 奈米波段提升了 2%, 我們認為這種奈米小球在紫外光波段可以當作反射鏡來使用.

Defect Passivation by Nanospheres Using H_3PO_4 and KOH Etching for UV LED

Student : Yin-Tsung Ma Advisor : Cheng-Chung Lin

Institute of Photonic System

National Chiao Tung University

Abstract

In this thesis, we compared defect passivation process by using H_3PO_4 and KOH etching solution. We observed GaN etching morphology.The H_3PO_4 prefer to etch screw type dislocation which is treated as non-radiative centers. On the other hand, KOH prefer to attack edge type dislocation.

We simplified the defect passivation process by using silica nanospheres as blocking material, which is much cheaper and convenience than using plasma-enhanced chemical vapor deposition.

By blocking the non-radiative centers, the internal quantum efficiency has been enhanced 17.1%.

The reflection of embedded silica nanospheres were enhanced about 2% in 361nm wavelength, which verified the silica nanosphere could act as reflector in ultraviolet.

致謝

兩年的碩士生涯是如此匆促，短暫但紮實的訓練讓我再踏入職場前更有信心去面對接下來的挑戰，研究所遇到的每個過去都是未來成熟的基石。

非常感謝我的指導教授林建中老師，他尤如是我碩士生涯領我進門的師傅，教導我成為碩士所需具備的一切，沒有他就沒有今天的我。再來是中研院的程育人博士，他猶如我另一個指導教授般一步步帶領我走向最終的目的，對程博的感謝無法用言語來形容，他是一個非常好的老師。

在台南念書時是我人生中最美好的時光之一，威麟，磬礐，禹軒，一正，佩蓉，翊生，坤廷，品儀，彥中，在空曠的校園中有你們而充實。感謝竹君，我實驗上的第一個老師，你把我教的很好，感謝奇穎，你是最好的學長，也是我心中的榜樣。感謝玫君，尚樺，家楊，諮宜，士超，建廷，孟佑，孟勳，威慶，郁君，宗佑等中研院的各位，大家一起為將來奮鬥，大家一起打拼的感覺真的很好。感謝電子所的各位博閔，士邦，哲榮，昀瑾，祐誠，國彬，你們是我看過最強的團隊，沒有你們幫忙就沒有我的論文，期待你們的發光發熱。啟煌，沛豪兩

位學弟加油，相信你們很快就會完成你們的論文。

最後感謝我的家人，尤其是我的父母一直秉持著犧牲自己也要讓小孩接受最好教育的理念讓我非常感動，而我在今天完成了使命，相信往後會令你們更驕傲。

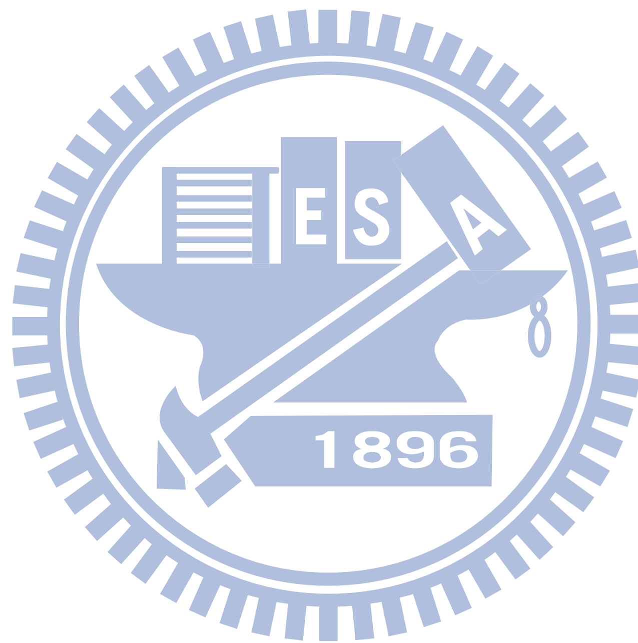

Contents

中文摘要……i
English Abstract……ii
Acknowledgment……iii
Content……v
Table Captions……vii
Figure Captions……viii
Chapter 1 Introduction……1
1.1 Review of III-nitrides development……1
1.2 Characteristics of Gallium Nitride(GaN)……2
1.3 Motivation……4
1.4 Reference……7
Chapter 2 Mechanism and Properties……11
2.1 The physical mechanisms for light emitting diodes……11
2.1.1 Internal quantum efficiency & Non-radiative recombination center...11
2.1.2 The limits of light extraction efficiency……14
2.2 Key issues for realizing high efficiency LEDs……18
2.2.1 Quality issues of GaN epitaxial layers……18
2.2.2 Light extraction of GaN LEDs……20
2.3 Wet etching……20
2.3.1 Defect properties on GaN surface……20
2.3.2 Etching process in molten KOH……22
2.4 Reference……27
Chapter 3 Measurement Systems……31
3.1 Scanning electron microscopy (SEM)……31
3.2 Cathodoluminescent spectroscopy (CL)……33
3.3 Atomic Force Microscopy (AFM)……34
3.4 Micro photoluminescence spectroscopy (μ-PL)……36
3.5 Reference……38
Chapter 4 Experiment Process ……39
4.1 Experiment process flow……39
4.2 GaN surface etching by phosphoric acid and molten KOH……39
4.3 Coating silica nanospheres on GaN etching surface……46
4.4 Regrowth InAlGaN LED structure……48
4.5 Reference……50
Chapter 5 Results and Discussion……51
5.1 Etching pits density analysis……51

5.2 Photoluminescence analysis..53
5.3 Cathodoluminescence analysis..56
5.4 Internal quantum Efficiency..58
5.5 Reflection analysis..59
Chapter 6 Conclusion...61

Table Captions

Table 2.3 Various chemicals etch GaN………...……...……………………………24
Table 4.4 The detail recipe and etching pits density of all process sample….…….49
Table 5.1 The EPD data of Bulk GaN and regrow LED surface……….………….53

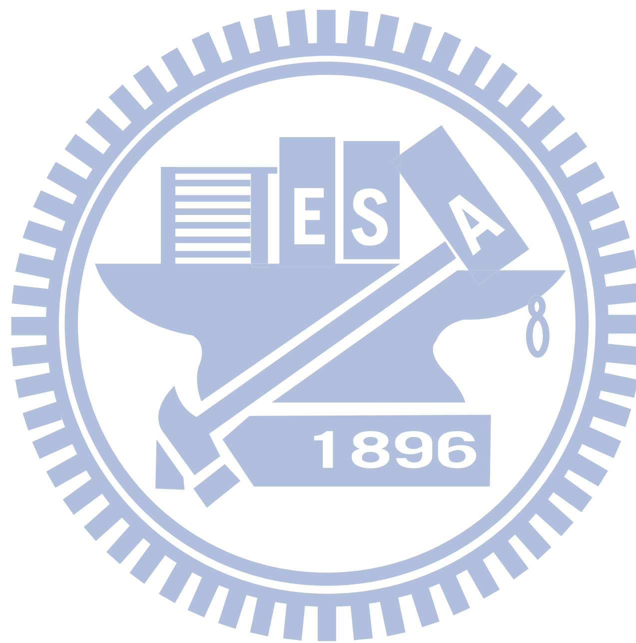

Figure Captions

Fig. 2.1.1 Schematic analogy carriers injected into active regions and depletion through radiative, nonradiative, and leakage recombinations……………………….16
Fig. 2.1.2 Radiative and non-radiative recombination in active region…………16
Fig. 2.1.3 (a) Cross section schematic diagram of typical LED structures (b) Photon trajectories inside the LED……………………………………………………...…16
Fig. 2.1.4 Total internal reflection in GaN-based LED……………………………16
Fig. 2.1.5 The angle of total internal reflection defines the light-escape cone………18
Fig. 2.3.1 Illustration of different polarity, (a) Ga-face (+c GaN, GaN polarity), (b) N-face (-c GaN, N-polarity)……………………………………………………….…25
Fig. 2.3.2 Schematic diagrams of the cross section GaN film viewed along [-1-120] direction for N-polar GaN to explain the mechanism of the polarity selective etching. (a) Nitrogen terminated layer with one negatively charged dangling bond on each nitrogen atom; (b) absorption of hydroxide ions; formation of oxides; (d) dissolving the oxides………………………………………………………………………..26
Fig. 3.1.1 Schematic diagram of a scanning electron microscope (SEM)…………...31
Fig. 3.1.2 Information that can be generated in the SEM by an electron beam striking the sample……………………………………………………………………………32
Fig. 3.2 JSM-7000F SEM and CL System……………………………………...33
Fig. 3.3 Operating mode of AFM (a) contact mode, (b) non-contact mode, (c) tapping mode………………………………………………………………………………36
Fig. 3.4.1 Inter-band transitions in photoluminescence system…………………37
Fig. 4.2.1 Bulk GaN surface etching test by (a)KOH and (b)H_3PO_4 solution…42
Fig. 4.2.2 The SEM image of GaN wet etching results, three etched pits types are observed……………………………………………………………………………43
Fig. 4.2.3 (a) Step formed at the beginning of etching screw type threading dislocation (b) A Ga face to prevent further vertical etching. (c) (d) Edge type threading dislocation was easily etching along the vertical dangling bond line……………….44
Fig. 4.2.4 GaN wafer etched by (a) KOH and (b) H_3PO_4……………………………45
Fig. 4.3.1 GaN wafer coating with 100nm silica nanopheres after etching process…46
Fig. 4.3.2 Nanosphere cleaning process with (a) and without (b) dust-free cloth wiping off the surface…………………………..……………………..…………...47
Fig.4.3.3 GaN wafer etched by KOHand H_3PO_4, then spin coating silica nanospheres with diameter 100nm. After cleaning process, the KOH sample (a) and H_3PO_4 (b) confined the nanospheres successfully…………………………………………....48
Fig. 4.4 Scheme of LED structure………………………………………………48

Fig. 5.1.1 SEM image of bulk GaN surface and LED surface after EPD test….52
Fig. 5.1.2 SEM image of LED cross section………………………………….…..52
Fig. 5.2.1 Photoluminescence spectrum of DSP LED……………………………..55
Fig. 5.2.2 Power Dependent PL Fitting of DSP LED……………………………..55
Fig. 5.3.1 CL measurement of DSP LED and Reference under quantum wavelength…………………………………………………………….………..57
Fig. 5.3.2 CL measurement of DSP LED and Reference under full wavelength….57
Fig. 5.4.1 The IQE results of LEDs………………………………………………..58
Fig. 5.5.1 Reflection of silica nanospheres embedded LED…………………………60
Fig. 5.5.2 Absorption of silica nanospheres embedded LED………………………...60

Chapter 1 Introduction

1.1 Review of III-nitrides development

For recent decades, III-nitride based light-emitting diodes (LEDs) in green, blue, and ultraviolet (UV) wavelength regions have been highly researched due to the wide direct band-gap and well thermal properties. The III-nitride compound material, such as InN、AlN can be alloyed with GaN has wide application in traffic signals、outdoor displays and back light in liquid- crystal displays.[1-7] The wurtzite structure of III-nitrides form an alloy system whose direct band-gap ranging from 0.7 eV for InN to 3.4 eV for GaN, and to 6.2 eV for AlN [8-9], the optical devices using III-nitrides could be activated at wavelength ranging from red to ultraviolet. Although the blue and green LEDs are commercially available[10-12], it is still difficult to manufacture high power ultraviolet GaN LEDs which can be acted as a pumping source for developing white LEDs[13], and the white LEDs can be the replacement of the conventional fluorescent lamp.

1.2 Characteristics of Gallium Nitride (GaN)

GaN is a direct and wide band-gap semiconductor commonly used in light-emitting diodes since the 1990s. This compound is a very stiff material that has a wurtzite crystal structure. Its wide band gap (3.4eV) will enable it special properties for applications in optoelectronics, high-power and high-frequency devices. For example, GaN is the substrate which makes violet (405 nm) laser diodes possible, without use of nonlinear optical frequency-doubling. Due to low sensitivity to ionizing radiation (like other group III nitrides), it is a suitable material for fabricating solar cell arrays for satellites (InGaN). Moreover, GaN transistors can operate at higher temperatures and work at much higher voltages than gallium arsenide (GaAs) transistors, which enable ideal power amplifiers at microwave frequencies.

GaN is a mechanically stable material with large heat capacity. In its pure form it resists cracking and can be deposited in thin film on sapphire or silicon carbide, despite the mismatch in their lattice constants. GaN can be doped with silicon (Si) or with oxygen to n-type and with magnesium (Mg) to p-type; however, the doping atoms change the way the GaN crystals grow, introducing tensile stresses and making them brittle. GaN compounds also tend to have a high spatial defect density, at the order of few hundred million to ten billion defects per square centimeter.

High crystal quality GaN has led to the commercialization of high-performance

blue LEDs and long-lifetime violet-laser diodes, and to the development of GaN-based devices such as UV detectors and high-speed field-effect transistors.

1.3 Motivation

Even though great progress has been made in the past few years, the GaN-based LED is still not as cost-effective as the traditional light source. One of the key issues is the low ouput power efficiency caused by defects or other problems during the epitaxial growth. In order to improve device performance, researchers are actively investigating various approaches. The overall performance of a LED can be decided by internal quantum efficiency and light extraction efficiency. The devices are often epitaxially grown on foreign substrates such as sapphire or silicon carbide (SiC) because a large-size commercial grade native substrate is still not available at a low cost. The as grown GaN epilayer has high threading dislocation (TD) density typically in the range of 10^{8}~10^{10} cm^{-2} owing to the mismatches in lattice constants and thermal expansion coefficients between GaN and sapphire. These defects are nonradiative recombination centers and are detrimental to optoelectronic device performance. For this reason, the reduction of TD is of great importance for the development of GaN based devices.

There are several epitaxial growth methods to improve crystal quality. A very commonly used one is the epitaxial lateral overgrowth technique (ELOG).[14-15] Strips of SiO_2 mask along specific crystal direction are deposited on GaN surface, followed by epitaxial growth. The growth starts from the window regions and grows

vertically as well as laterally to cover the SiO_2 strips until obtaining planar surface over whole wafer. The lateral growth above mask area bends the propagation direction of threading dislocation and results in significantly lower defect density. The defect density is, however, still high at window regions and coalescent boundaries. Another approach is to use patterned sapphire substrate for epitaxial growth,[16,17] but the reduction in TD defect density is often not as effective as ELOG method. Other methods use *in situ* SiN_x or *ex situ* TiN_x porous insertion layers,[18,19] where GaN nucleates from the pores of the inserted layer and lateral overgrowth on top of it. Recently, defect reduction methods using defect selective etching followed by metalorganic chemical vapor deposition (MOCVD)[20] or hydride vapor phase epitaxy[21] regrowth have also been reported.

In previous letter, *Lo et al.*[22] demonstrate a TD reduction method by self-aligned defect selective passivation (DSP) without the need of photolithography and use it to fabricate a high efficiency light emitting diodes (LED). The defect selective passivation is done by defect selective etching, SiO_2 passivation at etch pits, and epitaxial over growth.

However, this technique requires complicated processes and expensive equipment such as depositing the SiO_2 thin film by PECVD and removing the SiO_2 film on GaN surface by chemical mechanical polishing. In this study, we demonstrate the process

using silica nanospheres as a mask to block the propagation of TDs in GaN epitaxial layer growth. The process of selective defect passivation by self-assembled silica nanospheres was performed through a simple coating method and without photolithography patterning steps or expensive equipment. The process could reduce the density of threading dislocations by blocking the propagation of TDs.

1.4 Reference

[1]. S. Nakamura, T. Mukai, and M. Senoh, "high-brightness InGaN/AlGaN double-heterostructure blue-light-emitting diodes," *Appl. Phys. Lett.*, **67**, 1687 (1994)

[2]. S. Nakamura, M. Senoh, N. Iwasa, and S. Nagahama, "High-brightness InGaN blue, green and yellow light-emitting diodes with quantum well structures," Jpn. *J. Appl. Phys.*, **34**, L797 (1995)

[3]. G. Y. Xu, A. Salvador, W. Kim, Z. Fan, C. Lu, H. Tang, H. Markoc, G. Smith, M. Estes, B. Goldberg, W. Yank, and S. Krishnankutty, "High speed, low noise ultraviolet photodetectors based on GaN p-i-n and AlGaN(p)-GaN(i)-GaN(n) structures," *Appl. Phys. Lett.*, **71**, 2154 (1997)

[4]. T. G. Zhu, D. J. H. Lambert, B. S. Shelton, M. N. Wong, U. Chowdhury, H. K. Kwon, and R. D. Dupuis, "High-voltage GaN pin vertical rectifiers with 2 μm thick i-layer," Electron Lett., 36, 1971 (2000)

[5]. G. T. Dang, A. P. Zhang, F. Ren, X. A. Cao, S. J. Pearton, H. Cho, J. Han, J. I. Chyi, C. M. Lee, C. C. Chuo, S. N. G. Chu, and R. G. Wilson, "High Voltage GaN Schottky rectifiers," IEEE Trans. Electron Devices, 47, 692 (2000)

[6]. B. S. Shelton, D. J. H. Lambert, H. J. Jang, M. M. Wong, U. Chowdhury, Z. T. Gang, H. K. Kwon, Z. Liliental-Weber, M. Benarama, M. Feng, and R. D. Dupuis, "Selective area growth and characterization of AlGaN/GaN heterojunction bipolar

transistors by metalorganic chemical vapor deposition," IEEE Trans. Electron Devices, 48, 490 (2001)

[7]. A. P. Zhang, J. Han, F. Ren, K. E. Waldrio, C. R. Abernathy, B. Luo, G. Dang, J. W. Johnson, K. P. Lee, and S. J. Pearton, Electronchem. "GaN bipolar junction transistors with regrown emitters, " Solid-State Lett., 4, G39 (2001)

[8]. T. Matsuoka, H. Okamoto, M. Nakao, H. Harima, and E. Kurimoto, "Optical bandgap energy of wurtzite InN," Appl. Phys. Lett., 81, 1246 (2002)

[9]. H. Morkoc, "Nitride Semiconductors and devices," Springer-Verlag, Berlin, (1999)

[10] S. Nakamura and G. Fasol, "TheBlueLaserDiode.Berlin, Germany : Springer-Verlag," 1997, pp. 216–219.

[11] S. D. Lester, M. J. Ludowise, K. P. Killeen, B. H. Perez, J. N. Miller,and S. J. Rosner, "High-efficiency InGaN MQW blue and green LEDs," J. Cryst. Growth, vol. 189, pp. 786–789, 1998.

[12] S. Nakamura, T. Mukai, and M. Senoh, "Candela-class high-brightness InGaN/AlGaN double-heterostructure blue-light-emitting diodes," Appl. Phys. Lett., vol. 64, pp. 1687–1689, 1994.

[13]Y. Narukawa, I. Niki, K. Izuno, M. Yamada, Y. Murazki, and T. Mukai, "Phosphor-conversion white light-emitting diodes using InGaN near-ultraviolet chip," *Jpn. J. Appl. Phys. Lett.*, vol. 41, pp. L371–L373, 2002.

[14] T. Mukai, K. Takekawa, and S. Nakamura, "High-power long-lifetime InGaN/GaN/AlGaN-based laser diodes grown on pure GaN substrates," Jpn. J. Appl. Phys., Part 2 **37**, L839 (1998).

[15] O.-H. Nam, M. D. Bremser, T. S. Zheleva, and R. F. Davis, "Dislocation density reduction via lateral epitaxy in selectively grown GaN structures," Appl. Phys. Lett. **71**, 2638 (1997).

[16] E.-H. Park, J. Jang, S. Gupta, I. Ferguson, C.-H. Kim, S.-K. Jeon, and J.-S.Park, "Air-voids embedded high efficiency InGaN-light emitting diode," Appl. Phys. Lett. **93**, 191103 (2008).

[17] Y. J. Lee, H. C. Kuo, T. C. Lu, B. J. Su, and S. C. Wang, **"**Fabrication and Characterization of GaN -Based LEDs Grown on Chemical Wet-Etched Patterned Sapphire Substrates," J.Electrochem. Soc. **153**, G1106 (2006).

[18] J. Xie, Ü. Özgür, Y. Fu, X. Ni, H. Morkoç, C. K. Inoki, T. S. Kuan, J. V. Foreman, and H. O. Everitt, "Low dislocation densities and long carrier lifetimes in GaN thin films grown on a SiN_x nanonetwork," Appl. Phys. Lett. **90**, 041107 (2007).

[19] Ü. Özgür, Y. Fu, Y. T. Moon, F. Yun, H. Morkoç, H. O. Everitt, S. S. Park, and K. Y. Lee, "Long carrier lifetimes in GaN epitaxial layers grown using TiN porous network templates," Appl. Phys. Lett. **86**, 232106 (2005).

[20] J. W. Lee, C. Sone, Y. Park, S.-N. Lee, J.-H. Ryou, R. D. Dupuis, C.-H.

Hong, and H. Kim, “High efficiency GaN-based light-emitting diodes fabricated on dielectric mask-embedded structures,” Appl. Phys. Lett. **95**, 011108 (2009).

[21] J. L. Weyher, H. Ashraf, and P. R. Hageman, “Reduction of dislocation density in epitaxial GaN layers by overgrowth of defect-related etch pits,” Appl. Phys. Lett. **95**, 031913(2009).

Chapter 2 Mechanism and Properties

2.1 The physical mechanisms for light emitting diodes

2.1.1 Internal quantum efficiency & Non-radiative recombination center

For the double heterostructure active region, the injected current provides a generation processes as well as carrier leakage provides recombination term. The process of a certain steady-state carrier density in the active region could be compared to that a reservoir analogy, which is being simultaneously filled and drained, as shown in Fig. 2.1.1 In Fig. 2.1.1, there are $\eta_i = (\frac{I}{eV})$ electrons per second per unit volume being injected into the active region. The η_i, is the fraction of terminal current that generates carriers in the active region and V is the volume of active region.

Thus, the rate equation is determined as

$$\frac{dn}{dt} = G_{gen} - R_{rec} \tag{2-1}$$

where Ggen is the rate of injected electrons and Rrec is the rate of recombining electrons per unit volume in the active region. The recombination process is accompanied with spontaneous emission rate Rsp, nonradiative recombination rate Rnr, and carrier leakage rate Rl, as depicted in Fig. 2.1.1. Carrier leakage rate, R_l, is occurred when the transverse or lateral potential barriers are not sufficiently high. Thus, total recombination rate is expressed as below

$$Rrec = R_{sp} + R_{nr} + R_l \tag{2-2}$$

It is common to describe the natural decay processes by a carrier lifetime, τ. In the absence of photon generation term, the rate equation for carrier density is,

$$\frac{dn}{dt} = \frac{n}{\tau}, where \frac{n}{\tau} = R_{sp} + R_{nr} + R_l \tag{2-3}$$

The carrier rate equation in the equivalent be expressed as

$$\frac{dn}{dt} = Ggen - Rrec = (\frac{I}{eV}) - \frac{n}{\tau} \tag{2-4}$$

The spontaneous photon generation rate per unit volume is exactly equal to the spontaneous electron recombination rate, Rsp, since by definition every time an electron-hole pair recombines radiatively, a photon is generated. Under steady-state conditions, ($dn/dt = 0$), the generation rate equals the recombination rate,

$$(\frac{I}{eV}) = \frac{n}{\tau} = R_{sp} + R_{nr} + R_l \tag{2-5}$$

The spontaneously generated optical power, Psp, is obtained by multiplying the number of photons generated per unit time per unit volume, Rsp, by the energy per photon, $h\nu$, and the volume of the active region V. Then

$$P_{sp} = h\nu \times V \times R_{sp} = \eta_i \eta_r \frac{h\nu}{e} I \tag{2-6}$$

where the radiative efficiency, η_r, is defined as

$$\eta r = \frac{Rsp}{R_{sp} + R_{nr} + R_l} \tag{2-7}$$

Usually, the η_r depends on the carrier density and the product of $\eta i \eta_r$ is the internal efficiency, η_{int}. Thus according to Eq (2-6), the internal quantum efficiency

is defined as:

$$\eta_{\text{int}} = \frac{Psp/(h\nu)}{I/e} = \eta_i \eta_r \tag{2-8}$$

Internal quantum efficiency:

$$IQE = \frac{(the \quad number \quad of \quad photons \quad emitted \quad from \quad active \quad region \quad per \quad \text{sec}ond)}{(the \quad number \quad of \quad electrons \quad injected \quad \text{into} \quad LED \quad per \quad \text{sec}ond)} \tag{2-9}$$

Thus the internal quantum efficiency is related to η_i, the fraction of terminal current that generates carriers in the active region, and to η_r,the fraction of rates between radiative recombination to total carrier' recombination. According to Eq (2-8), we can enhance the internal quantum efficiency of LEDs by either increasing radiative recombination rate, R_{sp}, or decreasing nonradiative recombination rate, R_{nr}, and carrier leakage rate, R_l.

The possible recombinant paths of injected electrons and holes are shown in Fig. 2.1.2. Typically, material defect – including defects that extend over some distance of the material such as threading dislocation and more localized point defects such as vacancies and impurities – act as centers of nonradiaive recombination. Thus the overall goal in this stage is to enhance the radiative recombination rate and suppress the nonradiaive recombination rate. Therefore, significantly improvements of grown-layers quality associating with appropriate design of LEDs structure is the main thought to improve the internal quantum efficiency.

2.1.2 The limits of light extraction efficiency

A cross section schematic diagram of typical LED structures is shown in Fig. 2.1.3(a). The most serious problem with rectangular cubic may be that the photons generated at a point in the active region will be trapped inside the GaN and sapphire region as shown in Fig. 2.1.3(b), due to the continued total internal reflections off the chip wall as illustrated in Fig. 2.1.4. Assume that the angle of incidence in the semiconductor at the semiconductor-air interface is given by θ_1. Then the angle of incidence of the refracted ray, θ_2, can be derived from Snell's law

$$n_s \sin\theta_1 = n_a \sin\theta_2 \qquad (2\text{-}10)$$

Where, ns and na are the refractive indices of semiconductor and air, respectively. The critical angel θ_c for total internal reflection is obtained using θ_2=90°, using Snell's law, one obtains.

$$\sin\theta_c = \left(\frac{n_a}{n_s}\right)\sin 90°, \theta_c = \sin^{-1}\left(\frac{n_a}{n_s}\right) \qquad (2\text{-}11)$$

The angle of total internal reflection defines the light-escape cone as shown in Fig. 2.1.5. Light emitted into the cone can escape from the semiconductor, whereas light emitted outside the cone is suffered from total internal reflection. The surface area of the escape cone is given by the integral

$$Area = \int dA = \int_{\theta=0}^{\theta_c} 2\pi r \sin\theta_r d\theta = 2\pi r^2 (1-\cos\theta_c) \qquad (2\text{-}12)$$

Assume that light is emitted from a point-like source in the semiconductor with a

total power of Psource. Then the power that can escape from the semiconductor is given by

$$P_{escape} = P_{source} \frac{2\pi r^2 (1-\cos\theta_c)}{4\pi r^2} \quad (2\text{-}13)$$

Where $4\pi r^2$ is the entire surface area of the sphere with radius r. The calculation indicates that only a refraction of the light emitted inside a semiconductor can escape from the semiconductor. This fraction is given by

$$\eta_{ext} = \frac{P_{escape}}{P_{source}} = \frac{2\pi r^2 (1-\cos\theta_c)}{4\pi r^2} \quad (2\text{-}14)$$

Expanding Eq. (2-14) into power series and neglecting higher than second-order term yields

$$\eta_{ext} = \frac{1}{2}\left[1-\left(1-\frac{\theta_c^{\,2}}{2}\right)\right] = \frac{1}{4}\theta_c^{\,2} \approx \frac{1}{4}\frac{n_a}{n_s}, n_a = 1, n_s = n_{GaN} = 2.45 \quad (2\text{-}15)$$

According to Eq. (2-15), only a few percent (~4%) of the light generated in the semiconductor can escape from a planar LED.

ES A 1896

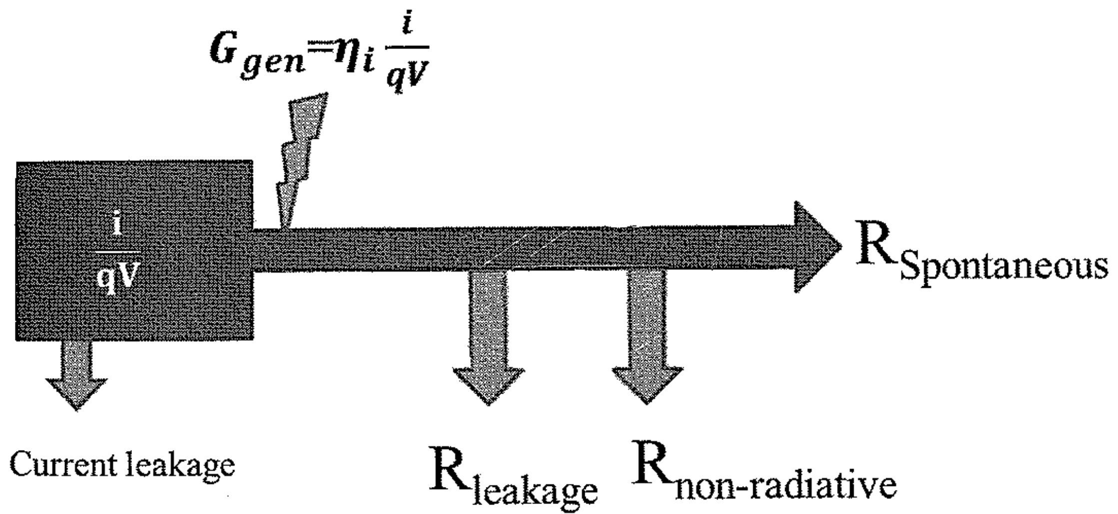

Fig. 2.1.1 Schematic analogy carriers injected into active regions and depletion through radiative, onradiative, and leakage recombinations. [21]

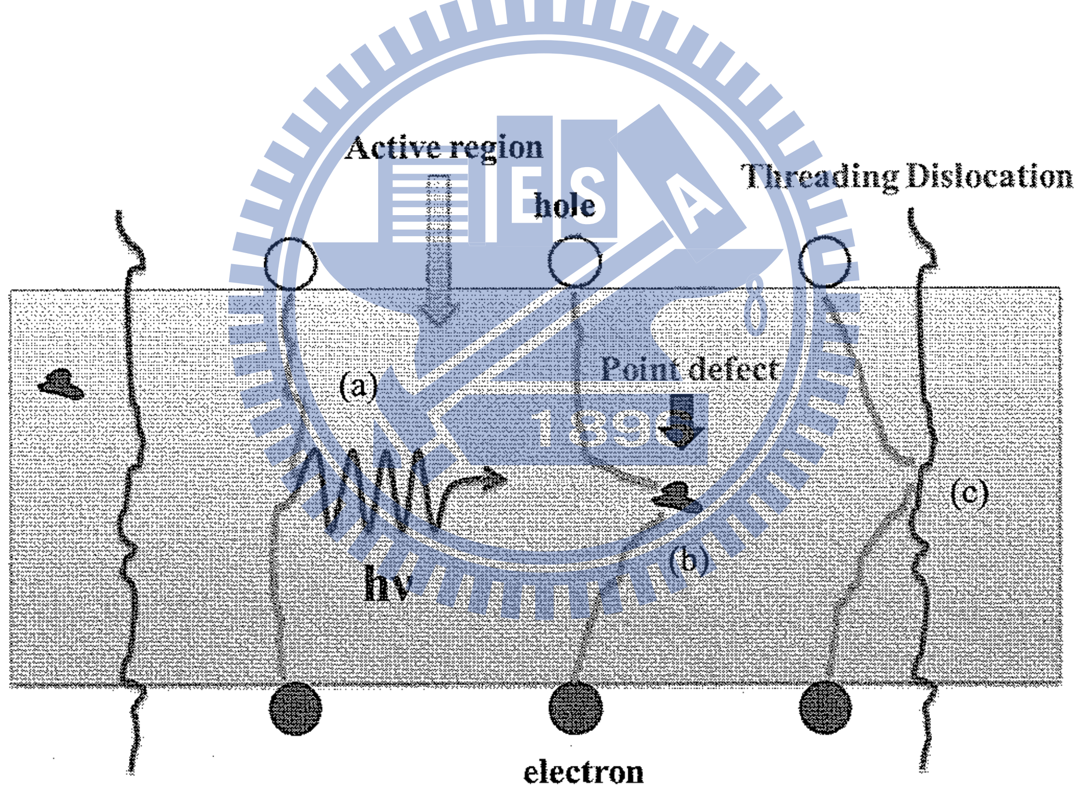

(a) Radiative path

(b) and (c) Non-radiative path

Fig. 2.1.2 Radiative and non-radiative recombination in active region. [21]

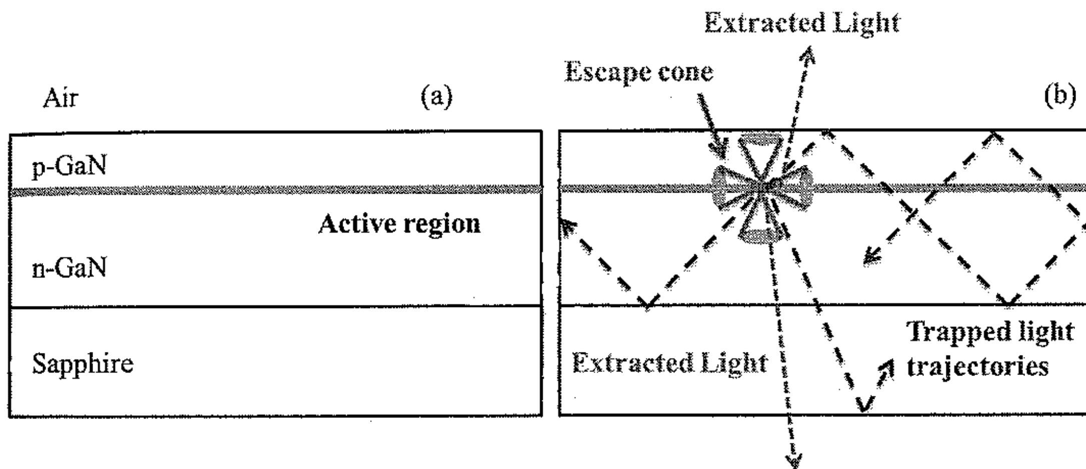

Fig. 2.1.3 (a) Cross section schematic diagram of typical LED structures (b) Photon trajectories inside the LED. [21]

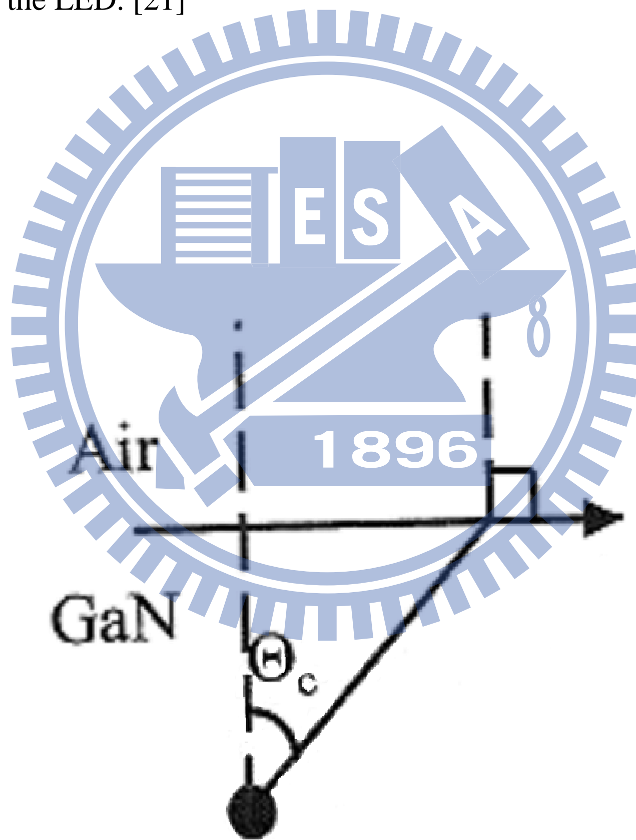

Fig. 2.1.4 Total internal reflection in GaN-based LED. [21]

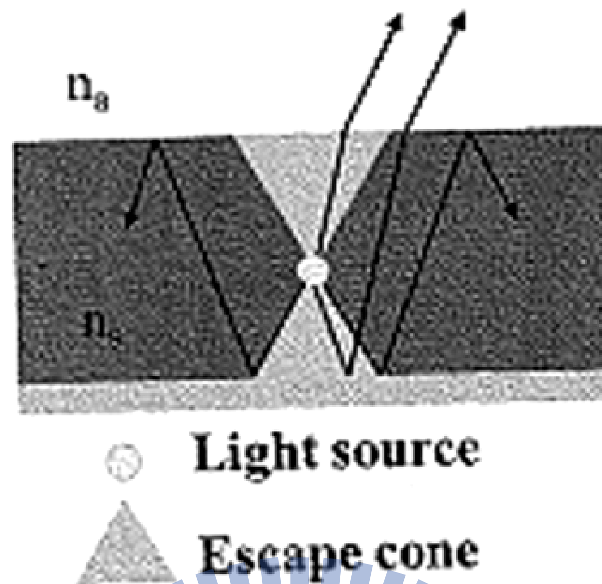

Fig. 2.1.5 The angle of total internal reflection defines the light-escape cone. [21]

2.2 Key issues for realizing high efficiency LEDs

2.2.1 Quality issues of GaN epitaxial layers

The GaN-based material and devices are often epitaxially grown on foreign substrate, such as silicon, silicon carbon (SiC) or sapphire. These substrates must be used because wafers of GaN are very expensive and not easily accessible like other common semiconductors. The nucleation layer, a layer grown at lower temperature, is used to initiate oriented growth on the substrate, followed by epitaxial growth on this layer at higher temperature. The as grown GaN epitaxial layer has high threading dislocation density (TDD) typically in the range of $10^{8-10}cm^{-2}$ due to the mismatched

in lattice constants (16%) and thermal expansion coefficients (39%) between GaN and sapphire, resulting in defect-mediated non-radiative recombination of electron-hole pairs and reduced mobility because of carriers trapped by the center of defect. These threading dislocation densities need to be drastically reduced because dislocations quench light emission of LEDs. These dislocation defects can be reduced by substrate patterning technique such as epitaxial lateral overgrowth (ELOG) [1], or pattern sapphire substrate [2], above approaches depend on spatial filtering, terminating, and turning of threading dislocation, so they do not reach the active region of active region. In this thesis, we report the defect passivation model to effectively block threading dislocation from the substrate to the active region. In particular, defect selective passivation structure not only block the propagation of threading dislocation, but also can act as light scattering sites to improve LEDs light extraction efficiency, similar to the use of patterned GaN/sapphire interface to reduce light trapped by total internal reflection.

2.2.2 Light extraction of GaN LEDs

Limitations in light extraction come from total internal reflection at interfaces and light absorption within the device or in the packaging. The generation of light in active region of an LED is most captured with GaN and sapphire by the guided modes. It is due to the high contrast refractive index at the GaN(n=2.45)/air(n=1) and GaN/sapphire(n=1.78) interfaces, resulting in total internal reflection that traps light in the high refractive index and in sapphire substrate. To improve the light extraction efficiency, there are several methods reported, such as patterned sapphire substrates, surface texturing, and air-void formation by nano-patterning.

2.3 Wet etching

2.3.1 Defect properties on GaN surface

Successful fabrication of GaN-based devices depends on the ability to grow epilayer on substrates such as sapphire or silicon carbide, with a low density of defects.[3,4] A high density (10^8~10^{10} cm^{-2}) of threading dislocations results from the lattice constant and thermal expansion coefficient mismatch in the nitride film.[5-7] We knew that these defects have influence on both the electrical and optical properties of the material.[8,9] Therefore, the availability of reliable and quick methods to investigate the defects and dislocations in GaN is of great interest.

Wet-chemical etching is a commonly used technique for surface defect investigation due to its advantage of low cost and simple experimental procedure. Hot phosphoric acid (H_3PO_4) and molten potassium hydroxide (KOH) have been shown to etch pits at defect sites on the c-plane of GaN.[10-13] The following segments was presented by P. Visconti and co-workers. Kozawa *et al.*[10] found etch pits tentatively ascribed to dislocations using molten KOH to etch metalorganic chemical-vapor deposition (MOCVD) GaN samples. However, the etch-pit density (EPD) was 2×10^7 cm^{-2}, while the dislocation density found by transmission electron microscopy (TEM) was 2×10^8 cm^{-2}. Hong and co-workers[11,12] related the hexagonal-shaped etch pits formed by H_3PO_4 etching on MOCVD GaN samples to nanopipes (open-core screw dislocations). EPD is hundreds or thousands times lower than the dislocation density evaluated by TEM. Lu[13] investigated etch pits formed on MOCVD GaN samples by molten KOH etching. By atomic-force microscopy (AFM) and TEM analyses, they attributed the origin of etch pits. Besides, the origin of etch pits is still controversial and the obtained EPD (in the range 4×10^5~1×10^8 cm^{-2}) is lower than the dislocation density (10^8~10^{10} cm^{-2}) found by TEM. The etch pits size varies even in the same sample. The shapes of etch pits are well correlated with types of defects, and the etch pits density (EPD) may correspond to the density of defects. However, for GaN, the density, types, and distribution of defects vary significantly due to growth-related

conditions, which makes it difficult to reach an agreement about the origin of the etch pits, and it can be even more difficult for test techniques.

2.3.2 Etching process in molten KOH

The discrepancy of etching characteristics in Ga-face (+c GaN, Ga-polarity) and N-face (-c GaN, N-polarity) has been specifically investigated as illustrated in Fig. 2.3.1. Some reports showed that gallium nitride could be etched in the aqueous sodium hydroxide (NaOH) solution but etching ceased when the formation of an insoluble coating of presumably gallium hydroxide ($Ga(OH)_3$) [14,15]. For further etching, it would need removing of the coating by continual jet action. Various aqueous acid and base solutions have been tested for etching of GaN were list in Table 2.3.1 [16-18]. The undetermined etch rate (nm/min) was because it various from sample to sample and differences in the defect density. According to the research reports in recent years; the common cognition related to gallium nitride etching process was that the most of gallium nitride could be etched rapidly in N-face. The reason for the face-dependent gallium nitride etching process has been studied by Li *et al.*, who utilized the X-ray photoelectron spectroscopy (XPS) to examine the surface chemistries before and after etching process in aqueous KOH solutions for both Ga- and N-face gallium nitride. The conclusion is that the different etching

results in Ga- and N-face gallium nitride crystals are due to the different states of surface bonding. Besides, the most important is the etching process only dependent on the polarities, not on the surface morphology, growth condition and which atoms form the surface termination layer. The GaN chemical etching reaction with KOH could be described as the following formula [19]:

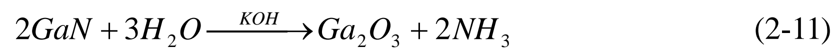

$$2GaN + 3H_2O \xrightarrow{KOH} Ga_2O_3 + 2NH_3 \quad (2\text{-}11)$$

Here, the molten KOH act as a catalyst and a solvent for the resulting Ga2O3 (Fig. 2.3.2 (d)) as well. The mechanism about etching N-face gallium nitride substrate was illustrated in Fig. 2.3.2. The hydroxide ions (OH^-) were first absorbed on the gallium nitride surface (Fig. 2.3.2 (b)) and finally react with Ga atoms once the OH^- ions with sufficient kinetic energy as shown in the Fig. 2.3.2 (c). The etching could be started at step (c) if the surface was Ga-terminated. The inertness of Ga-face GaN was ascribed to the hydroxide ions would be repelled by the negatively-charged triple dangling bonds of nitrogen near the surface. Thus, if the Ga-face GaN was Ga-terminated, the etching process stops after the first gallium atom layer was removed. In contrast, for the N-face GaN, every nitrogen atom bears a single dangling bond to prevent the hydroxide ions attacking from Ga atoms.

Table 2.3 Various chemicals etch GaN.[20]

Chemical	Temperature (°C)	Etch rate (μm/min)	Etching planes observed
Acetic acid (CH_3COOH)	30	<0.001	None
Hydrochloric acid (HCl)	50	<0.001	None
Nitric acid (HNO_3)	81	<0.001	None
Phosphoric acid (H_3PO_4)	108–195	0.013–3.2	$\{10\bar{1}\bar{2}\},\{10\bar{1}3\}$
Sulphuric acid (H_2SO_4)	93	<0.001	None
Potassium hydroxide (KOH), molten	150–247	0.003–2.3	$\{10\bar{1}0\},\{10\bar{1}\bar{1}\}$
50% KOH in H_2O	83	<0.001	None
10%–50% KOH in ethylene glycol (CH_2OHCH_2OH)	90–182	0.0015–1.3	$\{10\bar{1}0\}$
50% NaOH in H_2O	100	<0.001	None
20% NaOH in ethylene glycol	178	0.67–1.0	None

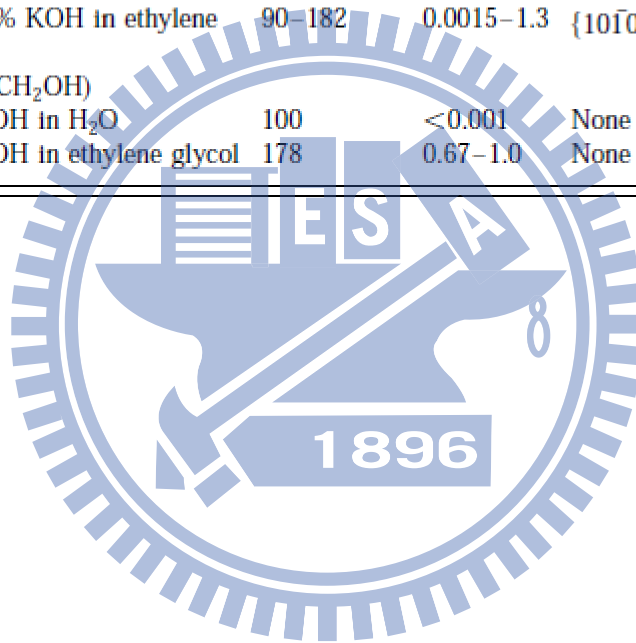

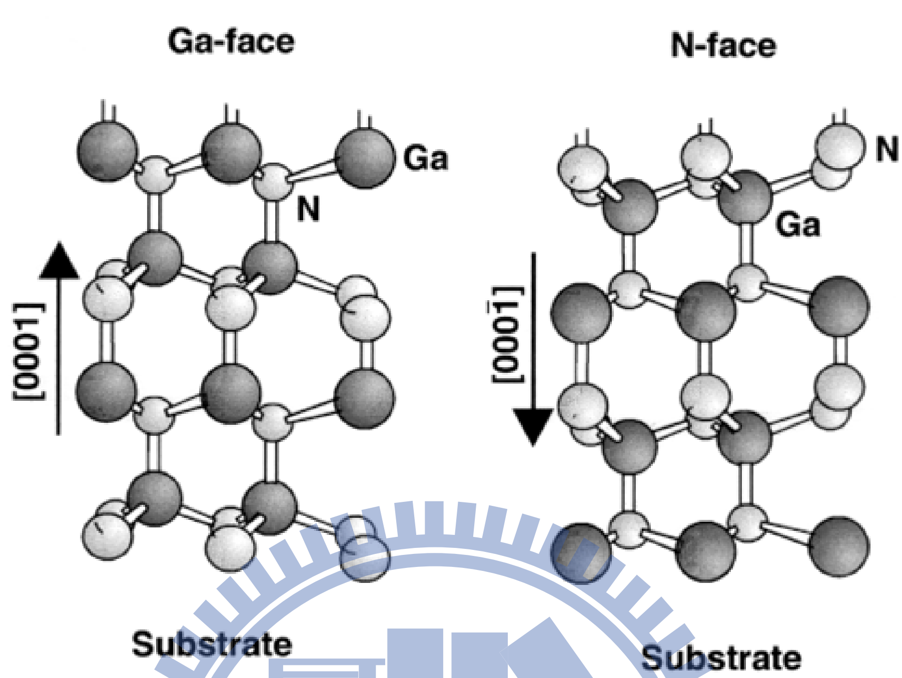

Fig. 2.3.1 Illustration of different polarity, (a) Ga-face (+c GaN, GaN polarity), (b) N-face (-c GaN, N-polarity). [22]

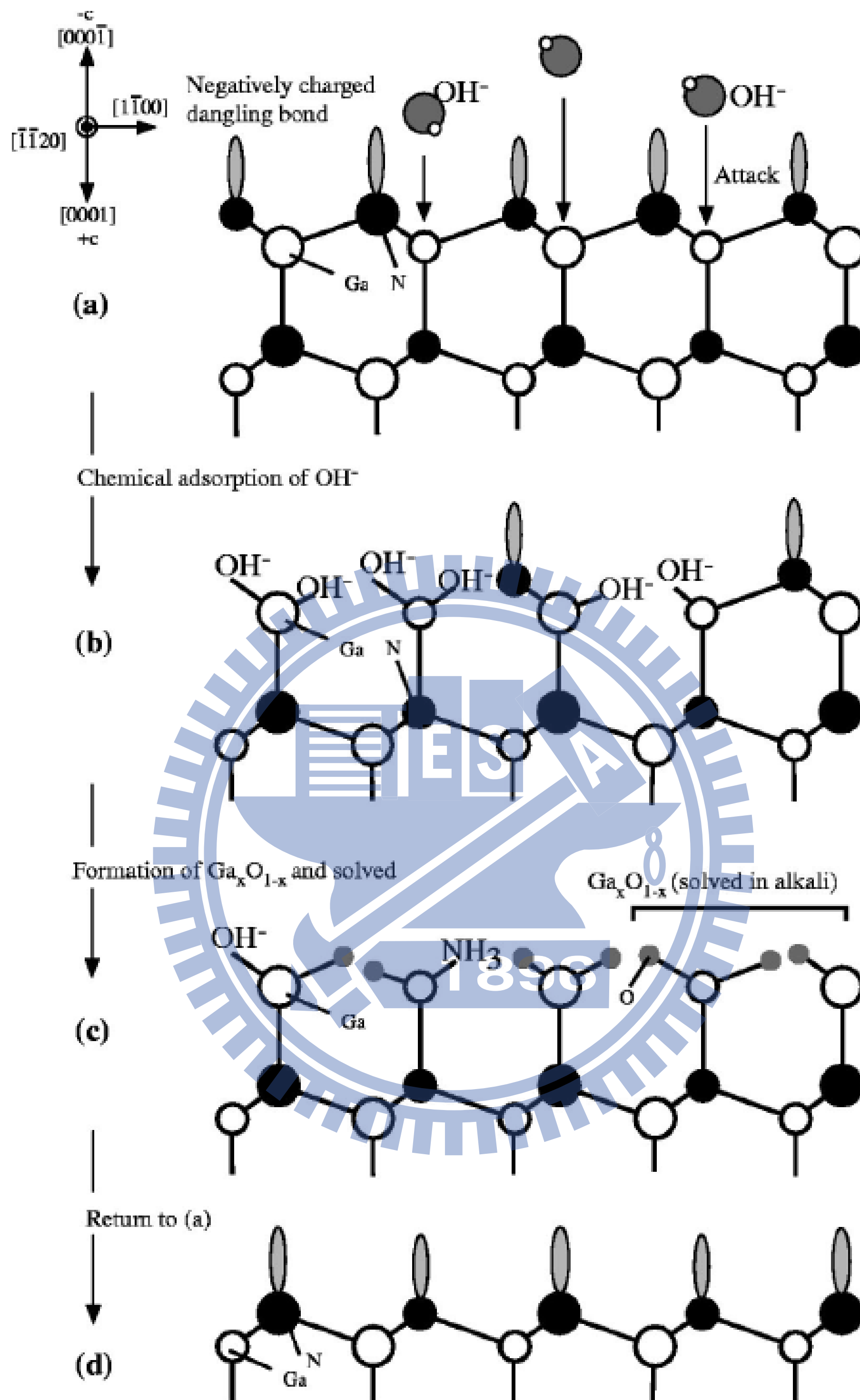

Fig. 2.3.2 Schematic diagrams of the cross section GaN film viewed along [-1-120] direction for N-polar GaN to explain the mechanism of the polarity selective etching. (a) Nitrogen terminated layer with one negatively charged dangling bond on each nitrogen atom; (b) absorption of hydroxide ions; formation of oxides; (d) dissolving the oxides. [23]

2.4 Reference

[1] A. Usui, H. Sunakawa, A. Sakai and A. A. Yamaguchi, "Thick GaN epitaxial growth with low dislocation density by hydride vapor phase epitaxy," Jpn. *J. Appl. Phys*. **36**, L889 (1997).

[2] M. Yamada, T. Mitani, Y, Narukawa, S. Shioji, I. Niki, S. Sonobe, K. Deguchi, M. Sano and T. Mukai, "InGaN-based near-ultraviolet and blue-light-emitting diodes with high external quantum efficiency using a patterned sapphire substrate and a mesh electrode," Jpn. *J. Appl. Phys*. **41**, L1431 (2002).

[3] H. Morkoc¸, S. Strite, G. B. Gao, M. E. Lin, B. Sverdlov, and M. Burns, "Large-band-gap SiC, III-V nitride, and II-VI ZnSe-based semiconductor device technologies," *J. Appl. Phys.* **76**, 1363 (1994).

[4] S. Nakamura, T. Mukai, and M. Senoh, "Candela-class high-brightness InGaN/AlGaN double-heterostructure blue-light-emitting diodes," *Appl. Phys. Lett.*, **64**, 1687 (1994).

[5] S. D. Lester, F. A. Ponce, M. G. Craford, and D. A. Steigerwald, "High dislocation densities in high efficiency GaN−based light−emitting diodes," *Appl. Phys. Lett.* **66**, 1249 (1995).

[6] W. Qian, M. Skowronski, M. DeGraef, K. Doverspike, L. B. Rowland, and D. K. Gaskill, "Microstructural characterization of α-GaN films grown on sapphire by

organometallic vapor phase epitaxy," *Appl. Phys. Lett.* **66**, 1252 (1995).

[7] X. H. Wu, L. M. Brown, D. Kapolnek, S. Keller, B. Keller, S. P. Den-Baars, and J. S. Speck, "Defect structure of metal−organic chemical vapor deposition−grown epitaxial (0001) GaN/Al_2O_3," *J. Appl. Phys.* **80**, 3228 (1996).

[8] B. Garni, J. Ma, N. Perkins, J. Liu, T. F. Kuech, and M. G. Lagally, "Scanning tunneling microscopy and tunneling luminescence of the surface of GaN films grown by vapor phase epitaxy," *Appl. Phys. Lett.* **68**, 1380 (1996).

[9] S. J. Rosner, E. C. Carr, M. J. Ludowise, G. Girolami, and H. I. Erikson, "Correlation of cathodoluminescence inhomogeneity with microstructural defects in epitaxial GaN grown by metalorganic chemical-vapor deposition," *Appl. Phys. Lett.* **70**, 420 (1997).

[10] T. Kozawa, T. Kachi, T. Ohwaki, Y. Taga, N. Koide, and M. Koike, "Dislocation Etch Pits in GaN Epitaxial Layers Grown on Sapphire Substrates," J. Electrochem. Soc. **143**, L17 (1996).

[11] S. K. Hong, T. Yao, B. J. Kim, S. Y. Yoon, and T. I. Kim, "Origin of hexagonal-shaped etch pits formed in (0001) GaN films," Appl. Phys. Lett. **77**, 82 (2000).

[12] S. K. Hong, B. J. Kim, H. S. Park, Y. Park, S. Y. Yoon, and T. I. Kim, "Evaluation of nanopipes in MOCVD grown (0 0 0 1) GaN/Al_2O_3 by wet chemical

etching," J.Cryst. Growth **191**, 275 (1998).

[13] L. Lu, Z. Y. Gao, B. Shen, F. J. Xu, S. Huang, Z. L. Miao, Y. Hao, Z. J. Yang, G. Y. Zhang, X. P. Zhang, J. Xu, D. P. Yu, "Microstructure and Origin of dislocation etch pits in GaN epilayers grown by metal organic chemical vapor deposition," *J. Appl. Phys.*, **104**, 123525 (2008)

[14] T.L. Chu, "Gallium Nitride Films," J. Electrochem. Soc. 118, 1200 (1971).

[15] J.I. Pankove," Electrolytic Etching of GaN," J. Electrochem. Soc. 119, 1118 (1972).

[16] H. Cho, D.C. Hays, C.B. Vartuli, S.J. Pearton, C.R. Abernathy, J.D. MacKenzie, F. Ren, J.C. Zolper, "Wet chemical etching survey of III-nitrides," Mater. Res. Soc. Symp. Proc. 483, 265 (1998).

[17] C.B. Vartuli, S.J. Pearton, C.R. Abernathy, J.D. MacKenzie, F. Ren, J.C. Zolper, R.J. Shul, "Wet chemical etching survey of III-nitrides," *Solid-State Electron*. 41 (12), 1947 (1998).

[18] S.J. Pearton, R.J. Shul, Gallium nitride I, in: J. Pankove, T.D. Moustakas (Eds.), "The Properties of Hydrogen in GaN and Related Alloys," Semiconductor and Semimetals Series, vol. 50, Academic Press, New York, NY, p. **103** (1998).

[19] D. Li, M. Sumiya, S. Fuke, D. Yang, D. Que, Y. Suzuki, Y. Fukuda,

“Selective etching of GaN polar surface in potassium hydroxide solution studied by x-ray photoelectron spectroscopy,” *J. Appl. Phys.* **90**, 4219 (2001).

[20] D. A. Stocker, E. F. Schubert and J. M. Redwing, “Crystallographic wet chemical etching of GaN,” Appl. Phys. Lett., Vol. 73, No. 18, 2 November (1998).

[21] M. H. Lo, P. M. Tu, C. H. Wang, C. W. Hung, S. C. Hsu, Y. J. Cheng, H. C. Kuo, H. W. Zan, S. C. Wang, C. Y. Chang, and S. C. Huang, “High efficiency light emitting diode with anisotropically etched GaN-sapphire interface,” Appl. Phys. Lett,95 041109 (2009)

[22] O Ambacher, “REVIEW ARTICLE Growth and applications of Group III-nitrides,” J. Phys. D: Appl. Phys. 31 2653–2710 (1998)

[23] D. S. Li, H. Chen, H. B. Yu, H. Q. Jia, Q. Huang, and J. M. Zhou, “Dependence of leakage current on dislocations in GaN-based light-emitting diodes,” J. Appl. Phys., Vol. 96, No. 2, pp. 1111-1114, Jul. (2004)

Chapter 3 Measurement System

3.1 Scanning electron microscopy (SEM)

The scanning electron microscope is built of the following parts:

(i) The electron gun

(ii) The system of three-stage electromagnetic lens is used to demagnify (focus, condense) the electron beam diameter to 5~10 nm at the specimen.

(iii) Detectors may detect electrons, X-ray or cathodo-luminescent (CL) light.

(iv) The microscope column is evacuated to 10^{-5} torr.

Fig. 3.1.1 shows that schematic diagram of a scanning electron microscope (SEM). Two pairs of deflection coils are shown in the SEM column. This double deflection allows the scanning beam to pass through the final aperture. Four pairs are actually used, for double deflection in *x* and *y* directions.

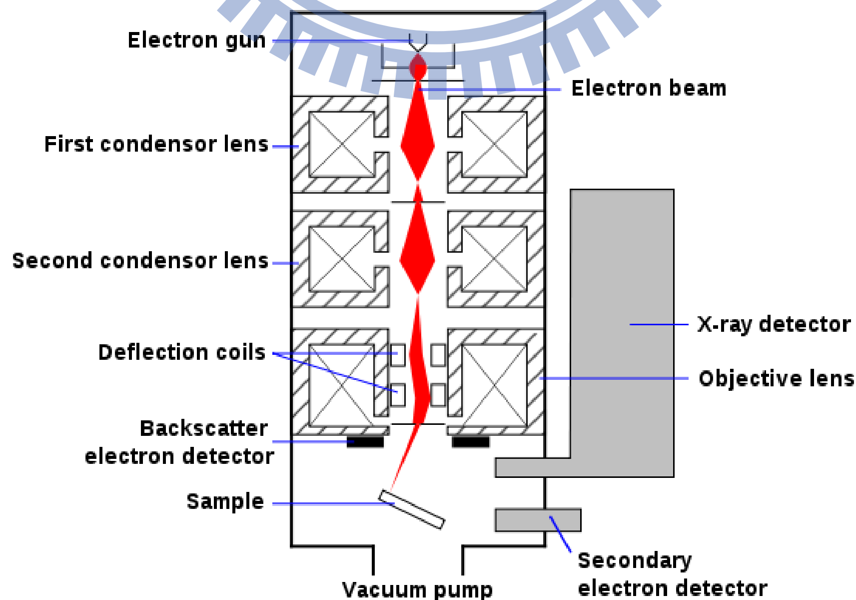

Fig. 3.1.1 Schematic diagram of a scanning electron microscope (SEM).[1]

SEM is a technique which forms an image of microscopic region of the specimen surface. An electron beam from 5~10 nm in diameter is scanned across the specimen. The interaction of the electron beam with the specimen produces a series of phenomena such as:

(i) backscattering of electrons of high energy

(ii) secondary electrons of low energy

(iii) absorption of electrons

(iv) X - ray

(v) visible light (cathodoluminescence, CL)

Fig. 3.1.2 indicates that any of these signals can be continuously monitored by detectors.

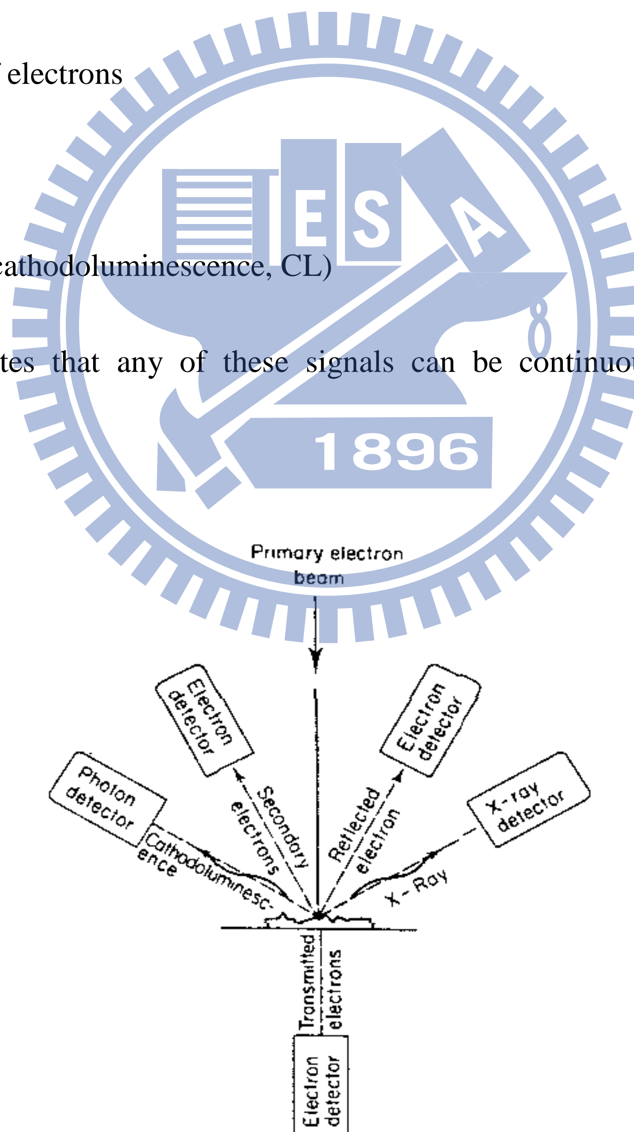

Fig. 3.1.2 Information that can be generated in the SEM by an electron beam striking

the sample.[2]

3.2 Cathodoluminescent spectroscopy (CL)

Cathodoluminescence (CL) is a SEM-based technique that can be used for analyzing the characteristic of semiconductor materials and devices. CL is the emission of light as the result of electron or “cathode-ray” bombardment. SEM-based and CL can provide information on the concentration and distribution of luminescent centers, distribution and density of electrically active defects, and electrical properties including minority carrier diffusion lengths and lifetimes.

Fig. 3.2 JSM-7000F SEM and CL System.

3.3 Atomic Force Microscopy (AFM)

Atomic force microscopy (AFM) or scanning force microscopy (SFM) is a very high-resolution type of scanning probe microscopy (SPM) instead of optical imaging one. In 1986, the AFM was invented by Gerd Binnig, Christoph Gerber, and Calvin F. Quate. The AFM is one of the foremost tools for imaging, measuring, and manipulating matter at the nanoscale. A very tiny, pyramidal probe is attached on the cantilever. The tip must be very tiny (single atom size) with sharp angle for large-area scan.

The AFM utilizes a sharp probe moving over the surface of a sample in a raster scan. When the probe is approaching sample surface, attractive (van der Waals force) or repulsive force (Coulomb repulsion) between tip and sample is formed and detected. Forces between the tip and the sample lead to a deflection of the cantilever according to Hooke's law. The interaction force causes cantilever to shift along z-axis and thus the topology of sample is obtained. The small probe-sample separation (on the order of the instrument's resolution) makes it possible to take measurements over a small area. To acquire an image the microscope-scans the probe over the sample while measuring the local property in question. The resulting image resembles an image on a screen in that both consist of many rows or lines of information placed on above the other. Unlike the traditional microscopes, scanned probe system do not use

lenses, so the size of the probe rather than diffraction effect generally limits their resolution.

Followings are the operating mode of AFM, shown as the Figs. 3.3[(a)-(c)]:

1. Contact mode: The Interaction mainly comes from repulsive force between tip and sample. It is easy to obtain atomic-scale resolution, but easy to damage surface of sample.
2. Non-contact mode: The Interaction mainly comes from van der Waals force between tip and sample. The tip never touches sample surface; resolution is lower (~50 nm). The surface of samples is preserved.
3. Tapping mode: The tip touches the surface of samples periodically. The resolution could be as high as contact-mode. The surface of samples could be damaged sometimes.

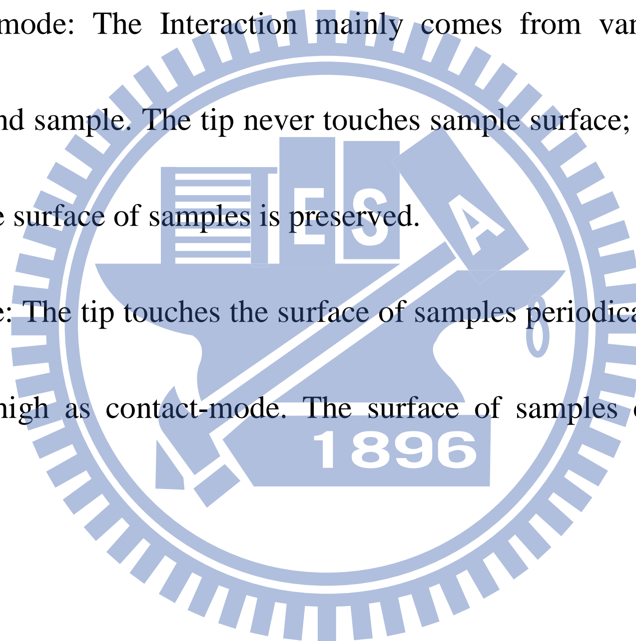

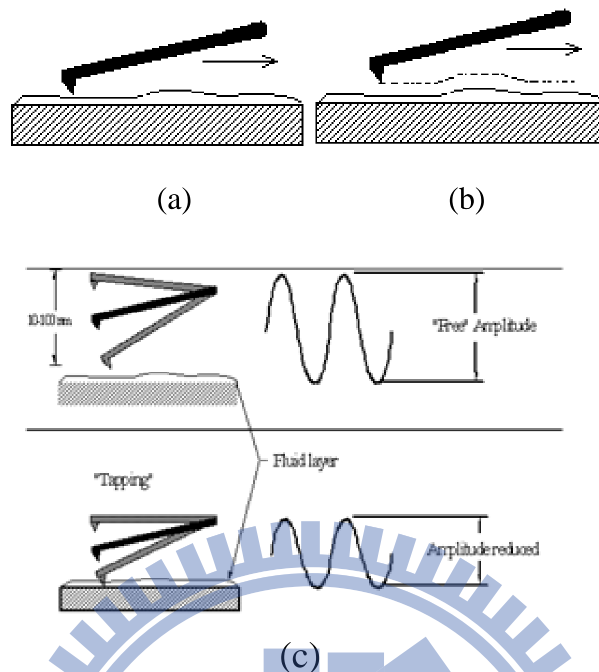

Fig. 3.3 Operating mode of AFM (a) contact mode, (b) non-contact mode, (c) tapping mode.[2]

3.4 Micro photoluminescence spectroscopy (μ-PL)

Photoluminescence (PL) spectroscopy has been used as a measurement method to detect the optical properties of the materials because of its nondestructive characteristics. PL is the emission of light from the material under optical excitation. Reducing the laser beam spot size to micrometer by beam expanders and objective lens is the so-called μ-PL. Fig 3.4.1 illustrates the photoluminescence process. The laser light source used to excite carriers should have large energy band gap than the semiconductors. When the laser light absorbed within the semiconductors, it should excite the carriers from the valence band to the conduction band. Then, is produces

the electrons in the conduction band and the holes in the valance band. When the electron in an excited state returns to the initial state, it will emit a photon whose energy is equal to energy difference between the excited state return and the initial state, therefore, we can observe the emission wavelength peak from PL spectrum.

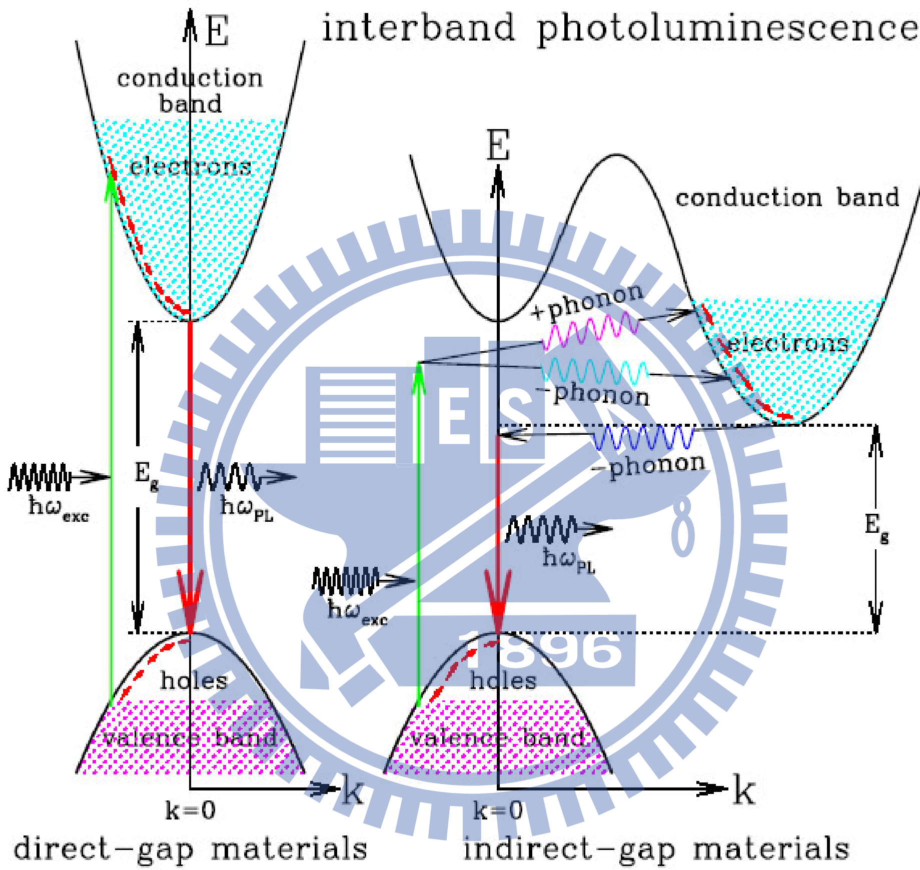

Fig. 3.4.1 Inter-band transitions in photoluminescence system.[3]

3.5 Reference

[1] http://en.wikipedia.org/wiki/File:Schema_MEB_(en).svg

[2] Class of Materials analysis, S. H. Yang, NCTU in Tainan

[3] http://ned.ipac.caltech.edu/level5/Sept03/Li/Li4.html

Chapter 4 Experiment Process

4.1 Experiment Process Flow

First, we reveal the bulk GaN pits of threading dislocation by chemical wet etching. Second, filling the defect pits by coating silica nanospheres. Finally, regrow UV LED structure.

In this thesis, we prepare two process samples and a bulk GaN sample as reference. One of the process sample use molten KOH as etching solution, while the other one use phosphoric acid. We observe the surface morphology and use optical measurement to analyze the epitaxial quality.

4.2 GaN surface etching by phosphoric acid and molten KOH

We verified that there are three types of etched pits：screw, edge, mixed (α, β, and γ) type [1]. Each etched pits correspond to different threading dislocations and threading dislocations having a screw component act as strong nonradiative centers [2], and the different etching liquid may forms different etched pit types. For this reason, a test round of the two GaN wafer was immersed in molten KOH and phosphoric acid (H_3PO_4), respectively.

The etching solution temperature and etching time dominate the pits size and

defect density. If the solution temperature or etching time is insufficient, it may lead to small pit size that is unable to confine the silica nanospheres in the pits. On the other hand, too much etching time or high solution temperature leads to larger pits size, which need to re-grow a thicker layer increasing the difficulty to seal the pits. Moreover, if the GaN is over-etched, the flat area of surface would be too fragile to provide the platform for re-growth. Therefore, it is important to find an appropriate recipe for etching process. As shown in fig. 4.2.1, the SEM image of GaN surface after etching by KOH and H_3PO_4. In the etching time versus temperature scheme, we chose 300°C 3 minutes for KOH and 240°C and 4 minutes for H_3PO_4 etching process. Both KOH and H_3PO_4 etching pits size are average about 1.2 um to 1.6 um, and the pit density is about 10^7 cm^{-2} and 10^6 cm^{-2} , respectively.

As shown in fig. 4.2.2, three etched pits type are observed. It is known that a screw type threading dislocation creates a step when it terminates at the GaN surface. In KOH etching process, these steps are easily attacked by OH^-, and further etching finally stop at the Ga terminate due to the chemical stabilization of Ga face as showed in fig. 4.2.3 [1]. Finally, the screw type threading dislocations can be etched to an inverse trapezoid. On the other hand, the edge type etched pits correspond to edge type threading dislocations. Since every atom in this line has dangling bond, the atom in this line was easily attacked, and finally formed a inversed pyramid. Mixed type

threading dislocations has both screw and edge type morphology.

Fig. 4.2.4 shows the top view SEM image of bulk GaN after etching test. The GaN etched by KOH revealed three types of etched pits. After calculating the etching pits density, we found that the edge type pits dominated KOH etching pits, the ratio of edge type pits is around 85%. On the other hand, We found only screw and mixed type etched pits in H_3PO_4 etching sample. The ratio of screw type and mixed type pits are around 95% and 5%, respectively.

In summary, we could infer that molten KOH prefer to etch edge type dislocation, while H_3PO_4 solution prefer to attack screw type dislocation, which is treat as non-radiative center[2]. In other words H_3PO_4 solution would much easier reveal non-radiative center than molten KOH.

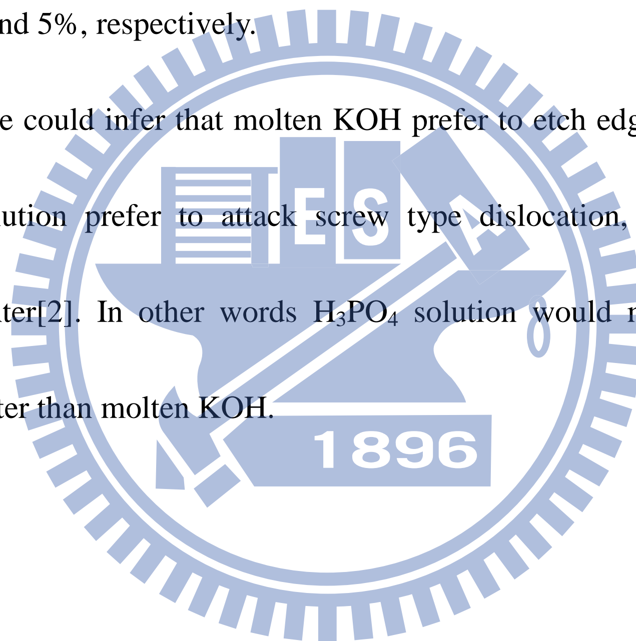

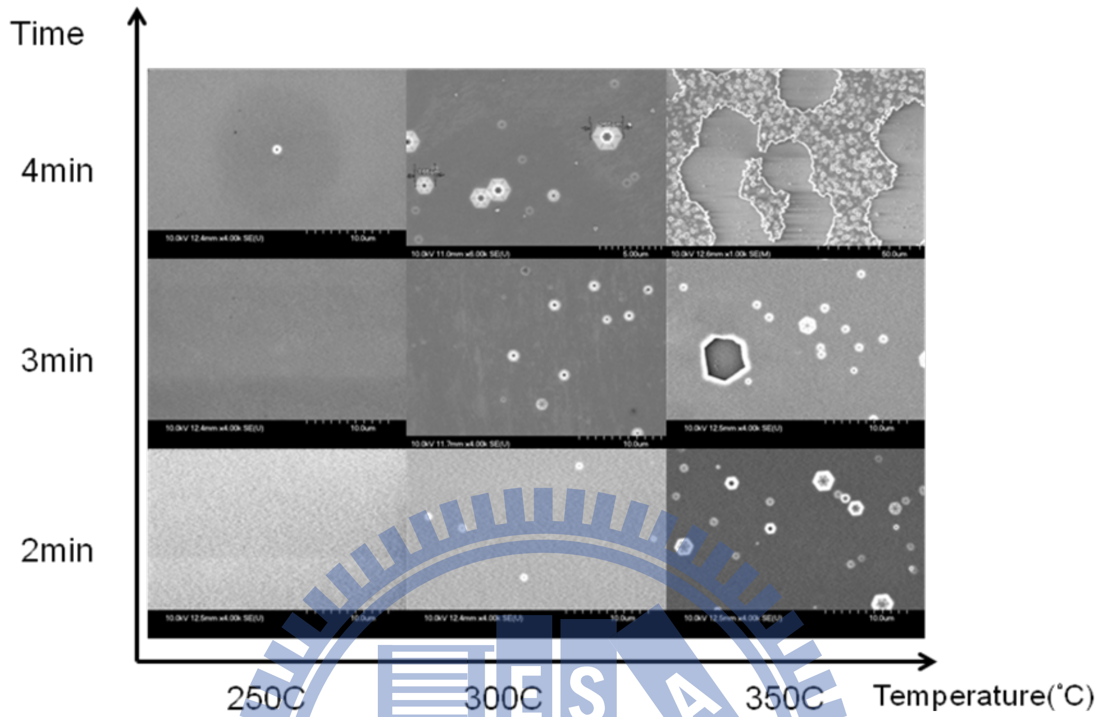

(a)

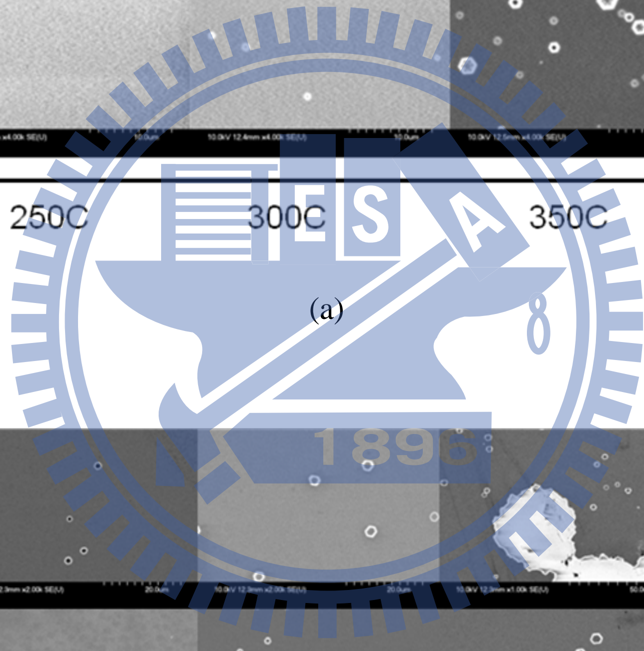

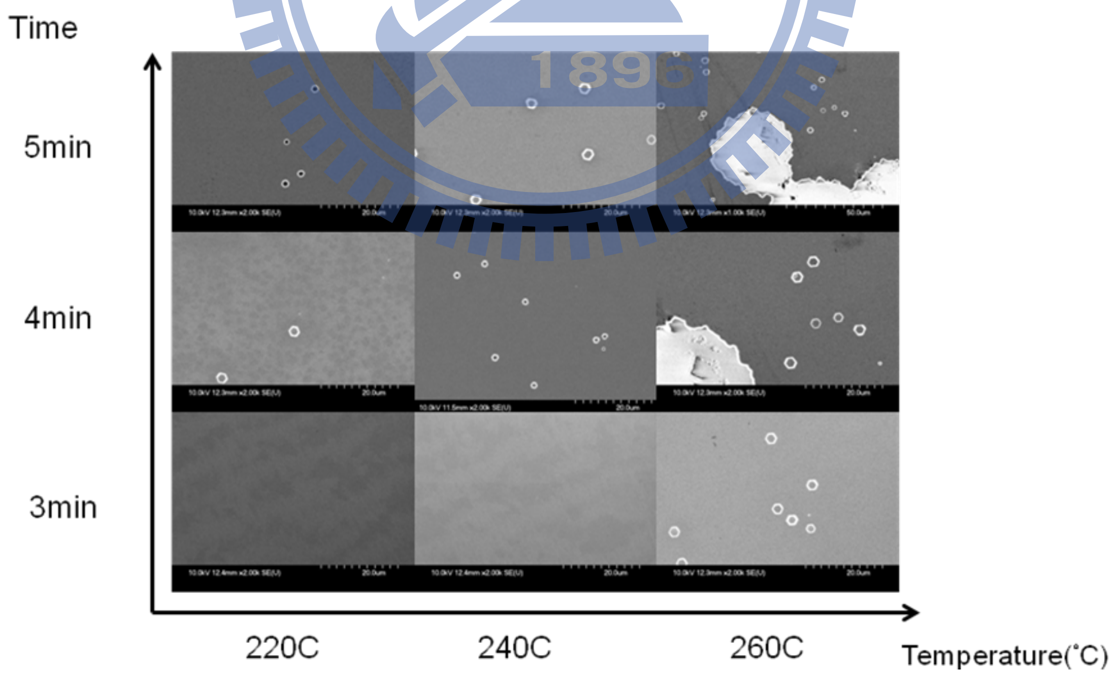

(b)

Fig. 4.2.1 Bulk GaN surface etching test by (a)KOH and (b)H_3PO_4 solution

Fig. 4.2.2 The SEM image of GaN wet etching results, three etched pits types are observed.

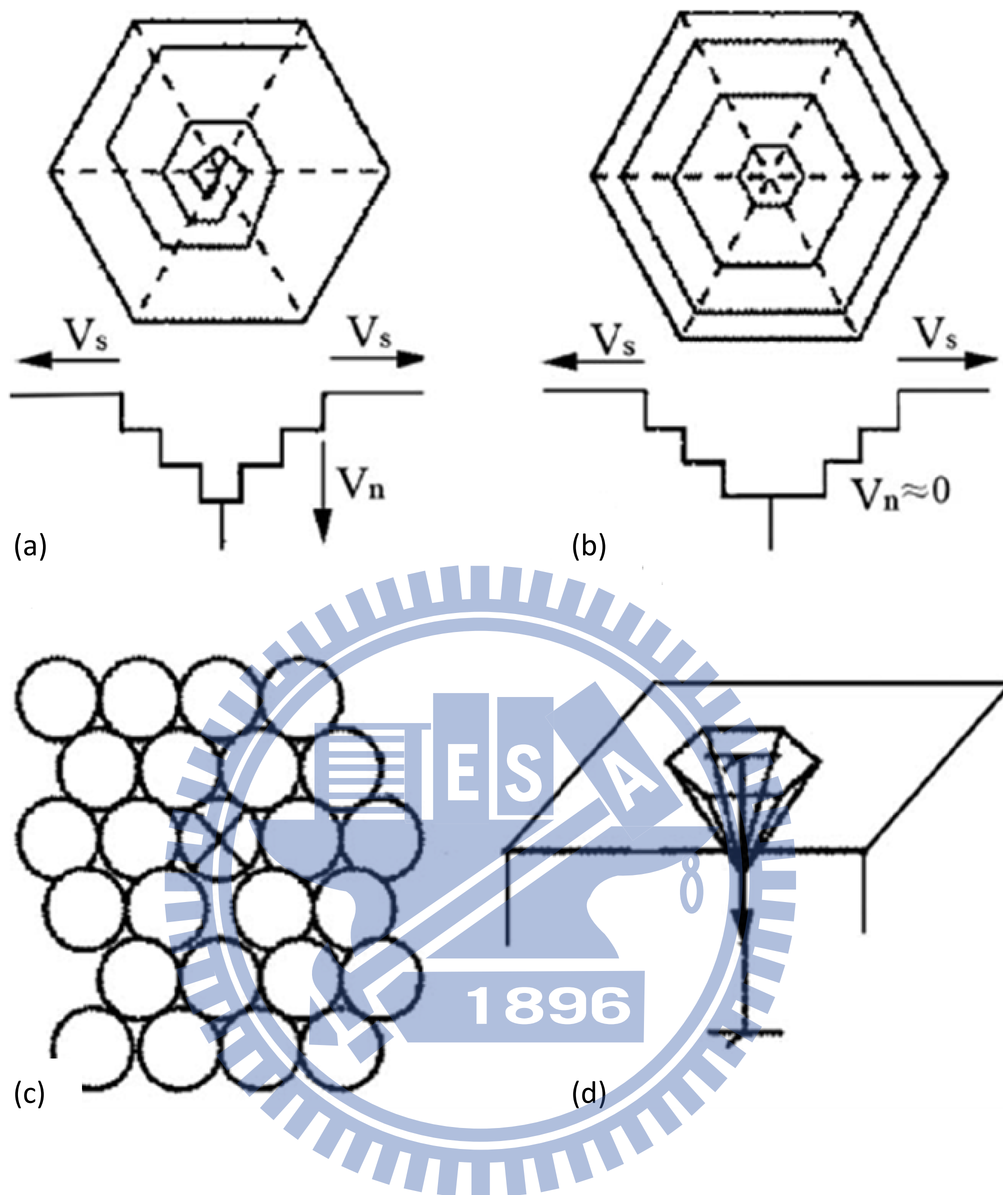

Fig. 4.2.3 [1] (a) Step formed at the beginning of etching screw type threading dislocation. (b) A Ga face to prevent further vertical etching. (c) (d) Edge type threading dislocation was easily etching along the vertical dangling bond line.

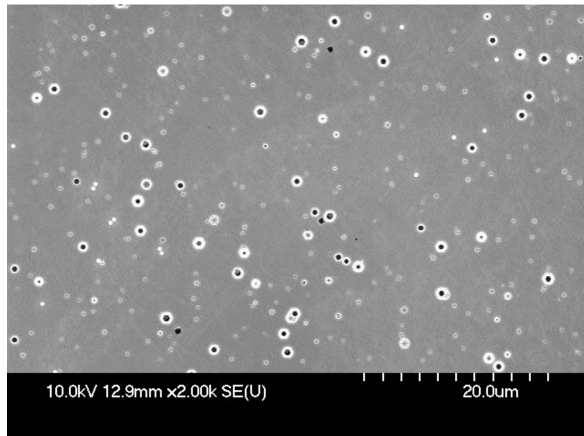

Defect type	Percentage
Edge	~85%
Screw	~3%
Mixed	~12%

(a)

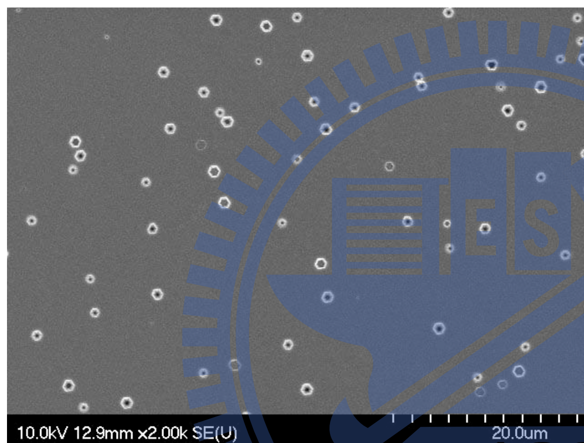

Defect type	Percentage
Edge	-
Screw	~95%
Mixed	~5%

(b)

Fig. 4.2.4 GaN wafer etched by (a)KOH and (b) H_3PO_4

4.3 Coating silica nanospheres on GaN etching surface

We coated diameters 100nm silica nanospheres on GaN surface after revealing the pits of threading dislocation. The SEM image is shown in fig. 4.3.1. Next step we removed the silica on the flat surface area and leaves silica nanspheres in the etching pits. The surface cleaning is the key issue. We wipe off the nanospheres on wafer surface by dust-free cloth, then clean by ultrasonic vibration in DI water for 5 minutes. Fig. 4.3.2 shows the difference between our clean process and without using dust-free cloth. The additional wiping process could totally remove the residual surface nanospheres.

Fig. 4.3.3 shows the GaN wafer after all cleaning process. We confined the silica nanospheres in etching pits successfully, and no nanospheres remained on surface.

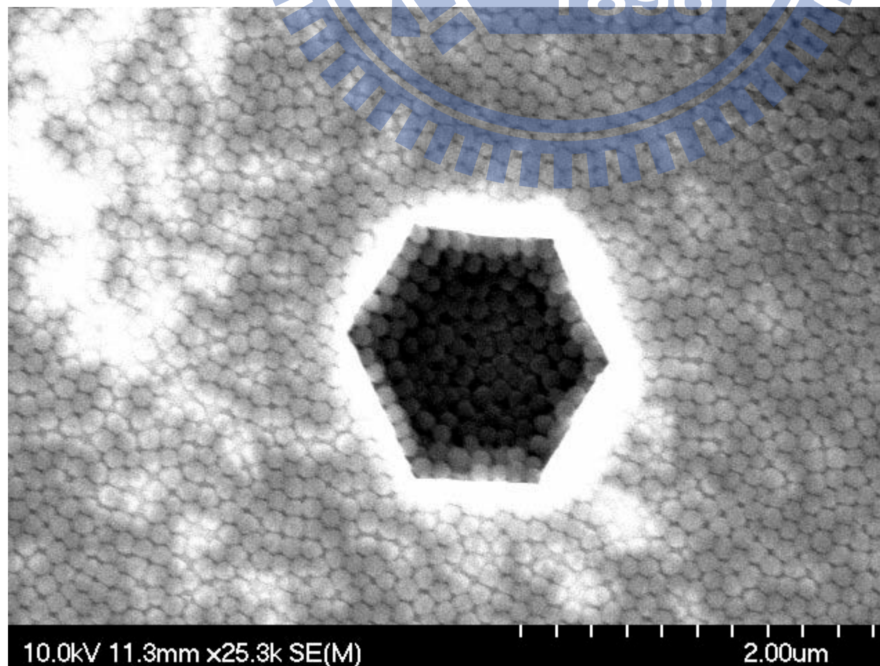

Fig. 4.3.1 GaN wafer coating with 100nm silica nanopheres after etching process.

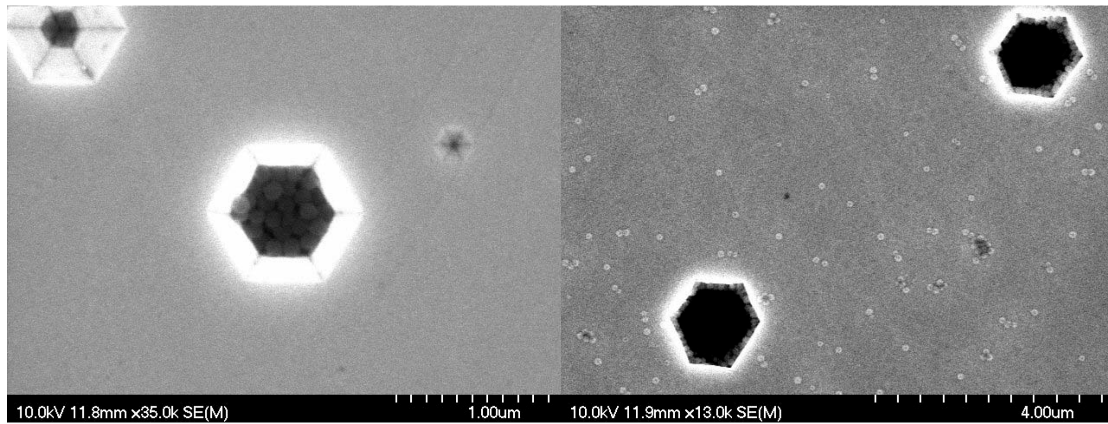

(a) (b)

Fig. 4.3.2 Nanosphere cleaning process with (a) and without (b) dust-free cloth wiping off the surface.

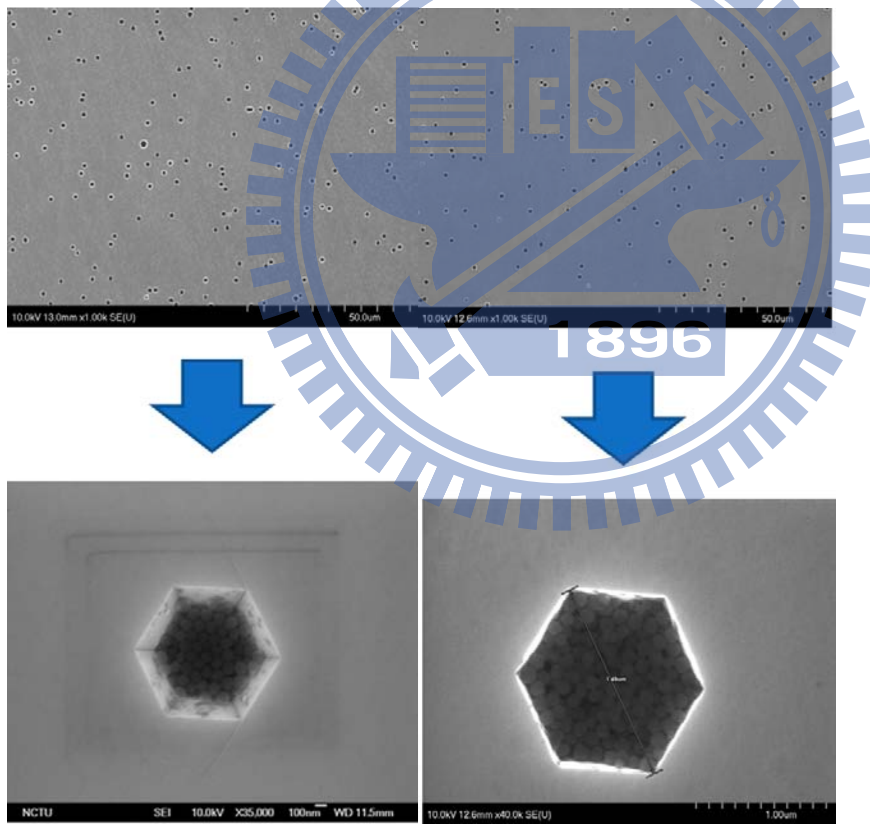

(a) (b)

Fig.4.3.3 GaN wafer etched by KOHand H_3PO_4, then spin coating silica nanospheres with diameter 100nm. After cleaning process, the KOH sample (a) and H_3PO_4 confined the nanospheres successfully.(b)

4.4 Regrowth InAlGaN LED structure

The InAlGaN based LED structure were regrown on all samples by using MOCVD. The LED structure are consisted of a 0.6um u-AlGaN layer, 2.04um n-InAlGaN layer. Ten pairs of InGaN/InAlGaN multiple quantum well active layer, 29.7nm AlGaN electron blocking layer, and a 55.6 nm p-GaN layer. The LED structure is showed in Fig. 4.4

The detailed parameters of all samples are shown in table 4.4.

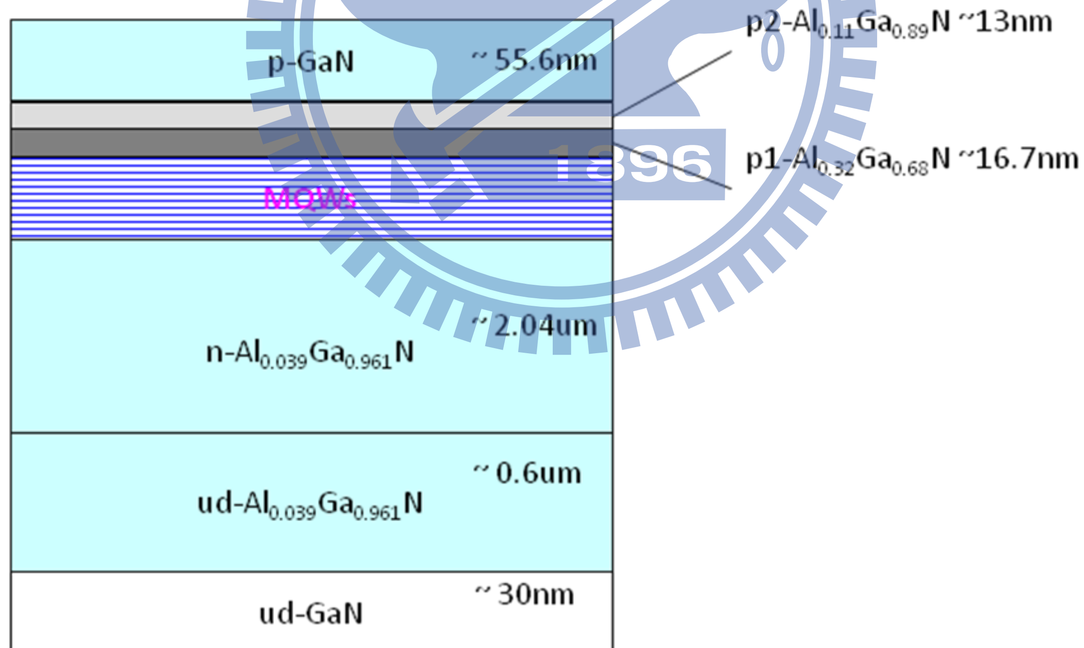

Fig. 4.4 Scheme of LED structure

Table 4.4 The detail recipe and etching pits density of all process sample

Sample	Ref	KOH	H3PO4
Etching solution	-	KOH	H3PO4
Etching time	-	3min	4min
Etching Pits Density(cm^{-2})	-	$1.6x10^{7}$	$4.25x10^{6}$
Coat Silica Size	-	100nm	100nm

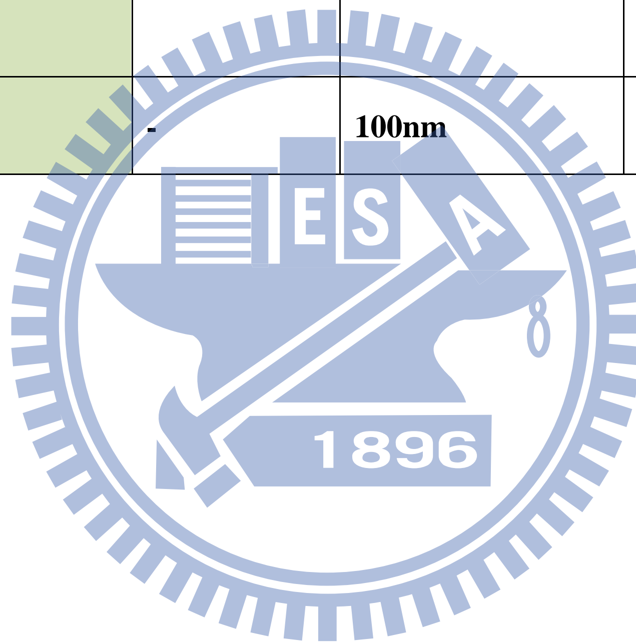

4.5 Reference

[1] L. Lu, Z. Y. Gao, B. Shen, F.J.Xu, S.Huang, Z. L. Miao, Y.Hao, Z. J. Yang, G.Y. Zhang, X. P. Zhang, J. Xu, and D. P. Yu "Microstructure and origin of dislocation etch pits in GaN epilayers grown by metal organic chemical vapor deposition," *J. Appl. Phys.*, **104**, 123525 (2008)

[2] T. Hino, S. Tomiya, T. Miyajima, K.Yanashima, S. Hashimoto, and M.Ikeda "Characterization of threading dislocations in GaN epitaxial layers," *Appl. Phys. Lett.*, **76**, 3421 (2000).

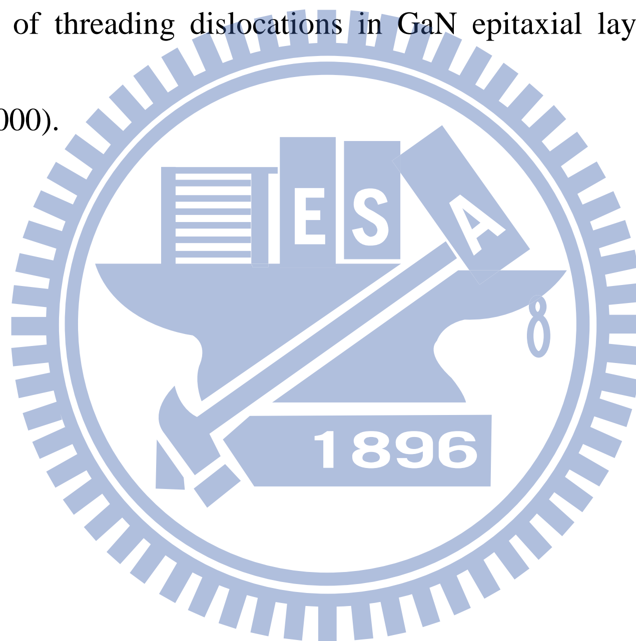

Chapter 5 Results and Discussion

5.1 Etching Pits Density analysis

To verify the quality improvement, we etched the p-GaN of LED for etching pits density (EPD) test again. Fig. 5.1.1 shows SEM image of the etched LED. We observe that the EPD decrease one order for KOH and two order for H3PO4 sample. This phenomenon attribute to the success of blocking threading dislocation. The detail EPD data are shown in table 5.1.

We used SEM observe the LED cross section area. The SEM image for H_3PO_4 and KOH is shown in Fig. 5.1.2. We could observe that the propagation of threading dislocation has been blocked, and it did not penetrate through the quantum well.

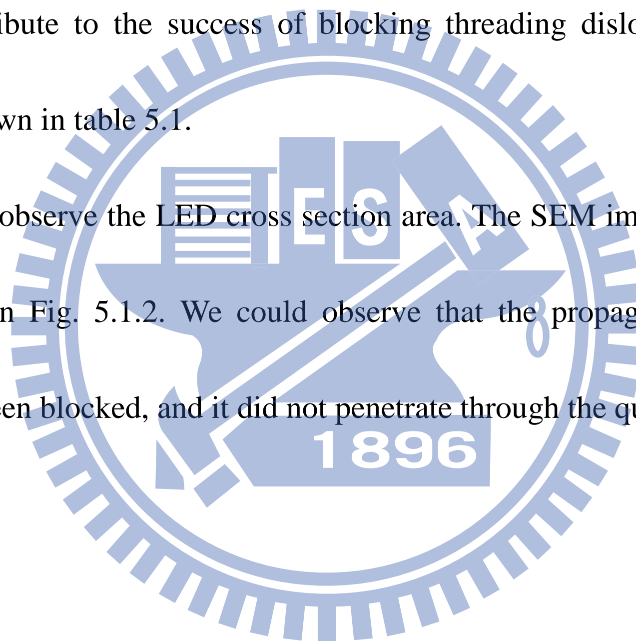

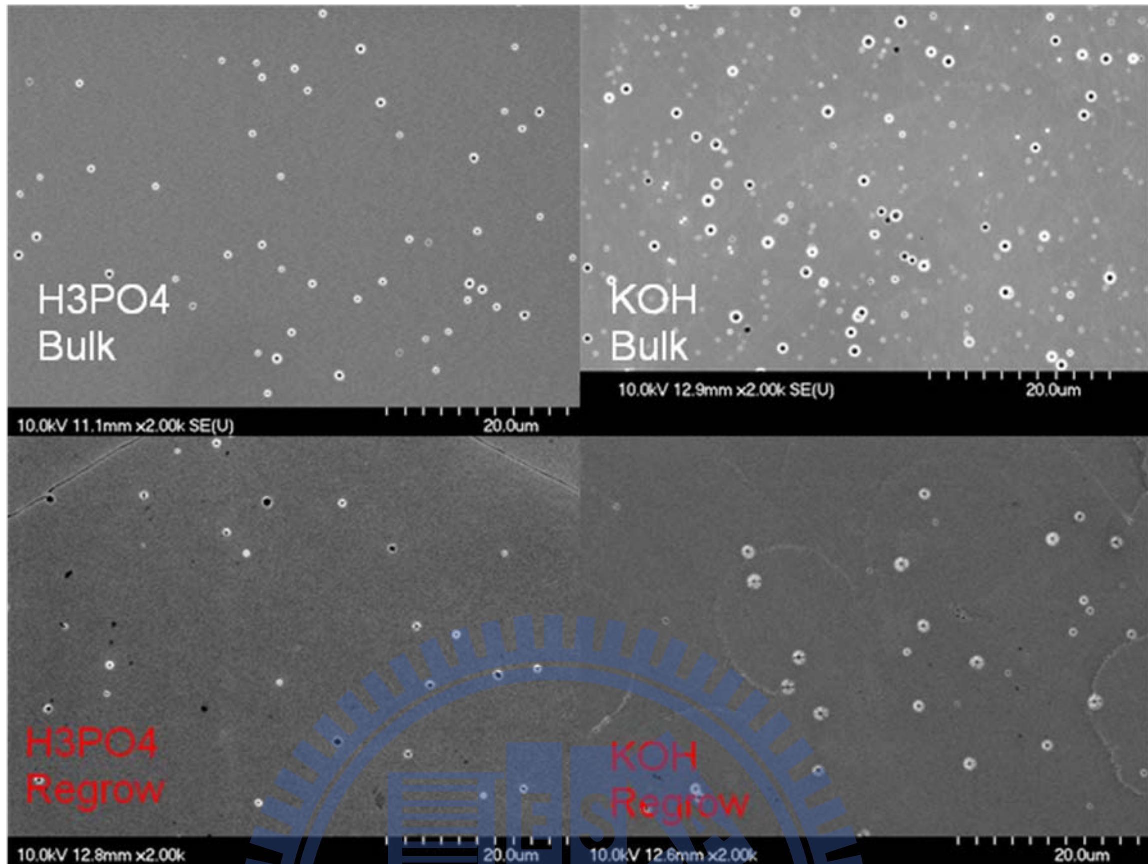

Fig. 5.1.1 SEM image of bulk GaN surface and LED surface after EPD test

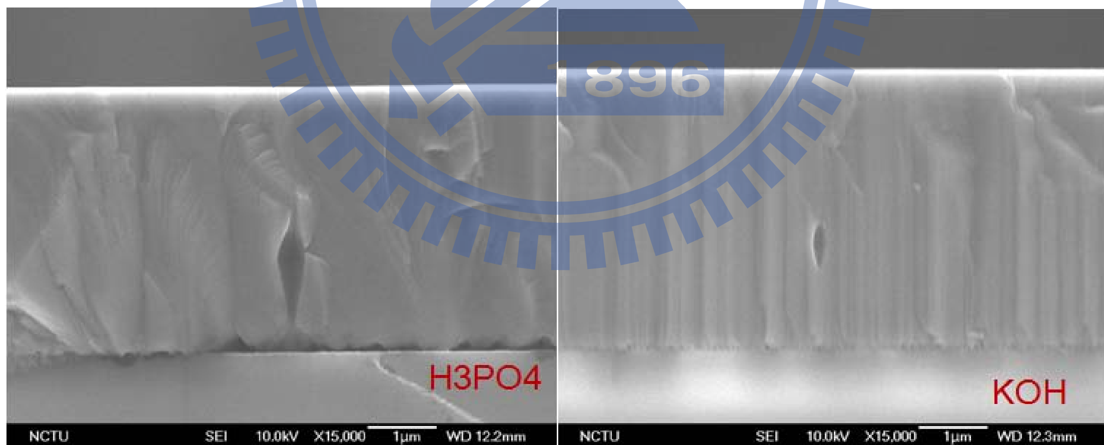

Fig. 5.1.2 SEM image of LED cross section

Table 5.1 The EPD data of Bulk GaN and regrow LED surface

EPD(cm^{-2})	Bulk	Regrow
H3PO4	$4.25x10^6$	$1.25x10^5$
KOH	$1.6x10^7$	$3.75x10^5$

ES A 1896

5.2 Photoluminescence analysis

Fig. 5.2.1 shows the room temperature PL of the regrow LED. The peak emission intensity (361nm) of the H3PO4 sample exhibited three times up than the other sample. We infered that the enhancement could be attributed to fewer defects and fewer non-radiative centers, which would trap the photo-generated carriers. The non-radiative center as well as screw type dislocation had been block by silica nanosphere and led to the strong emission phenomenon.

On the other hand, The KOH sample which prefer to attack edge type dislocation

did not exhibit a obvious enhancement. As mention in 4-2, the edge type pits dominate the KOH etching morphology, which is not non-radiative center.

We fitted the power dependent PL spectrum, and the H3PO4 sample exhibits a great enhancement compared to reference. The fitting results is shown in Fig. 5.2.2.

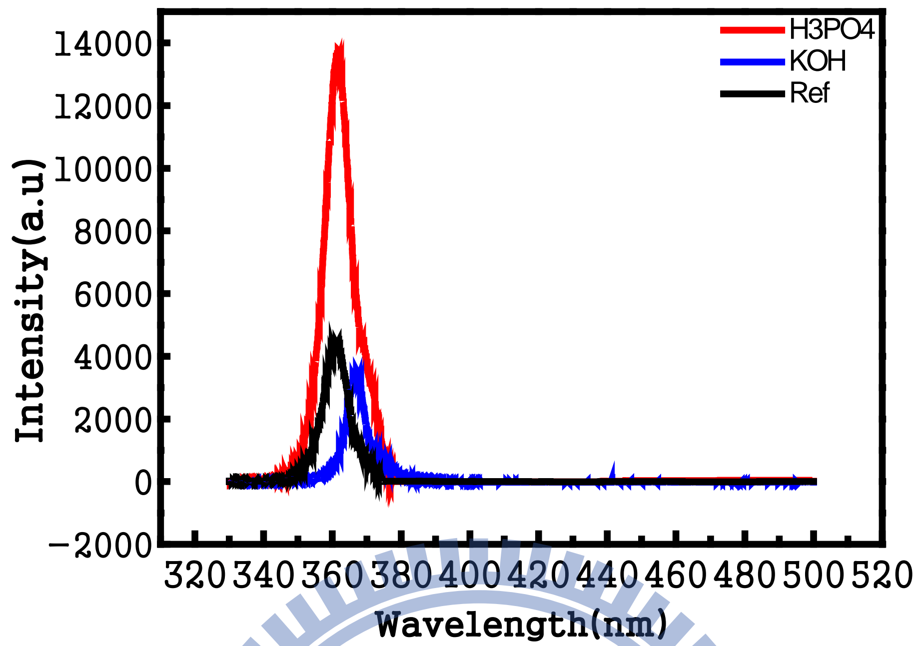

Fig. 5.2.1 Photoluminescence spectrum of DSP LED

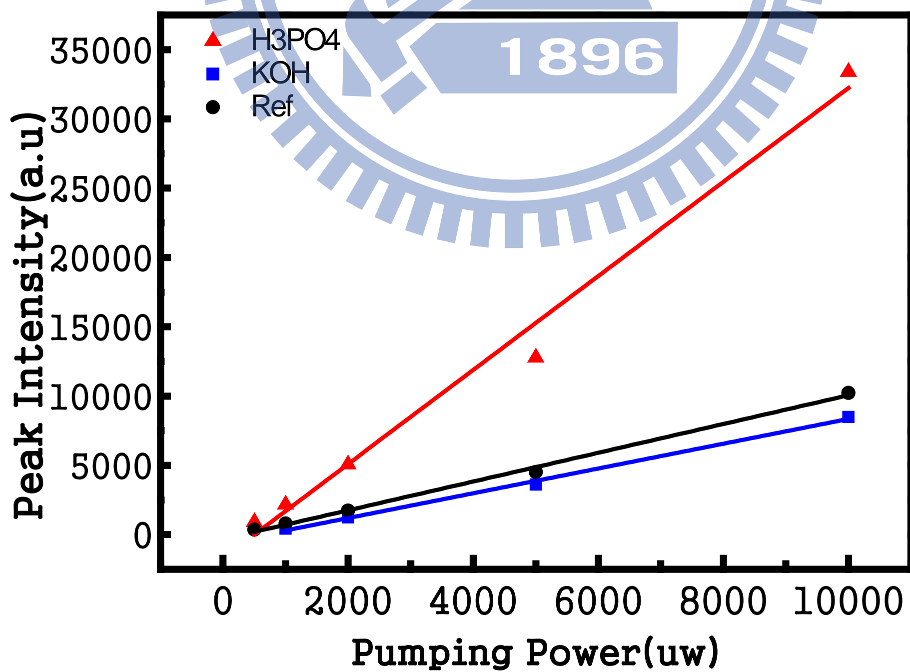

Fig 5.2.2 Power Dependent PL Fitting of DSP LED

5.3 Cathodoluminescence analysis

The optical characteristic is investigated by SEM and cathodoluminescence(CL) images as shown in Fig. 5.3.1. The image was taken under the quantum well emission wavelength as well as 361nm. The results implied the H3PO4 sample exhibited larger and more uniform luminescence area, which is showed less non-radiative center. We could infer that the material quality of H3PO4 sample has been improved. However, the KOH sample quality was decreased for some reason. The decrease may due to the epitaxial process problem.

We also analyze the CL spectrum under full wavelength with PMT 750 volt. The intensity trend was in agreement with PL measurement. The results showed in Fig. 5.3.2

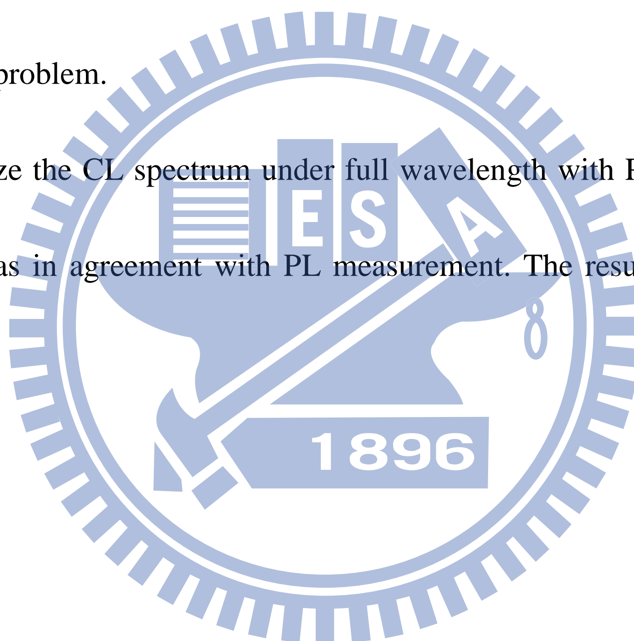

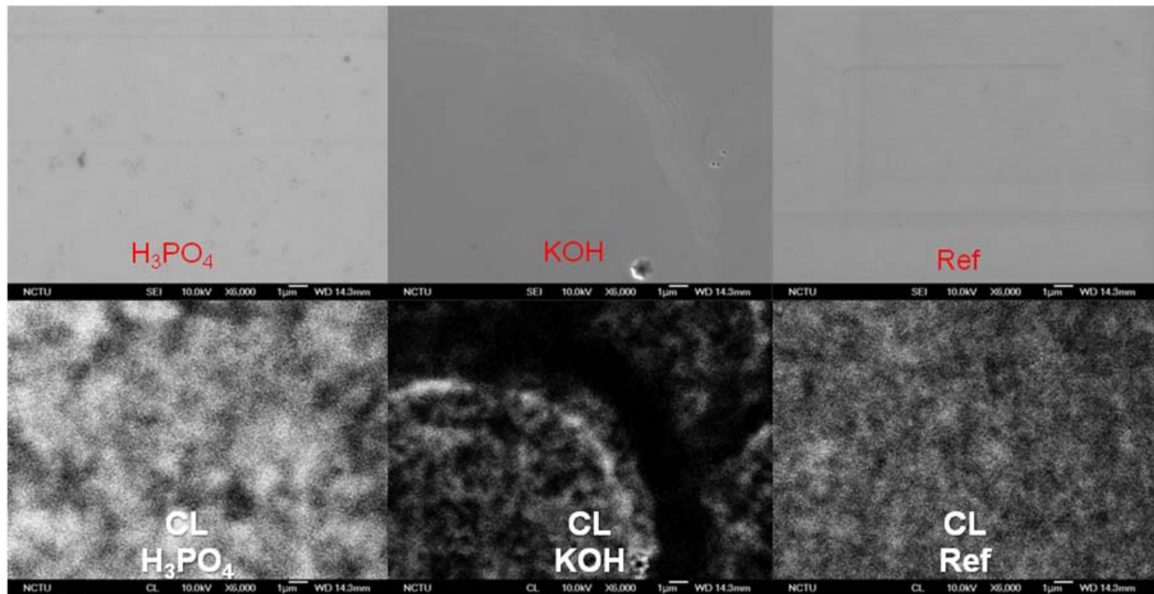

Figs. 5.3.1 CL measurement of DSP LED and Reference under quantum wavelength

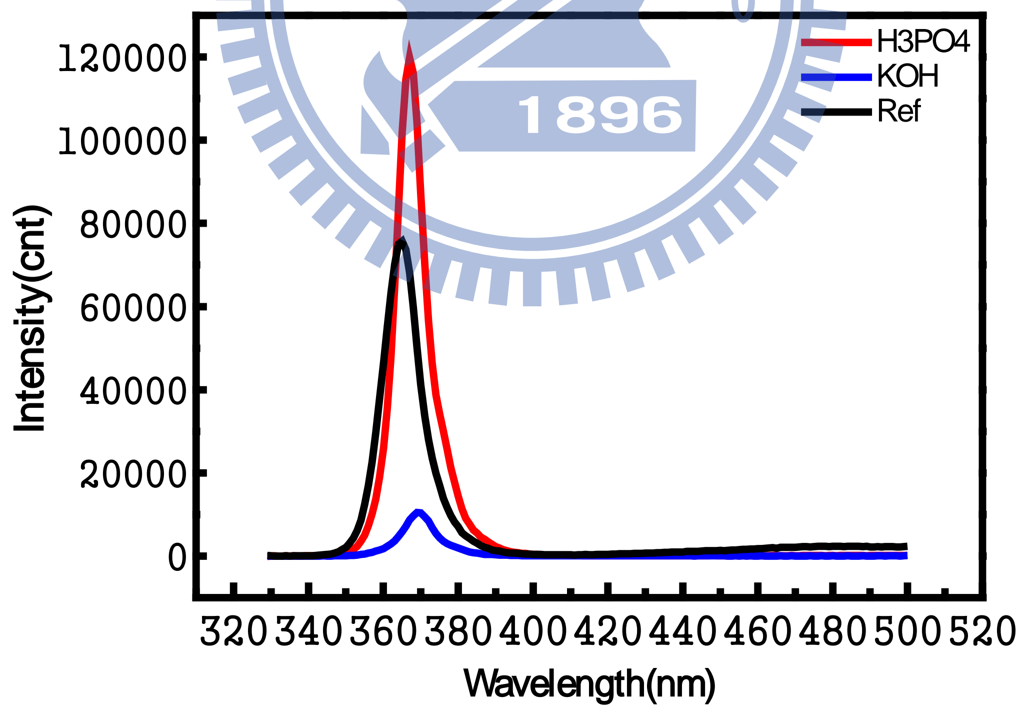

Fig. 5.3.2 CL measurement of DSP LED and Reference under full wavelength

5.4 Internal quantum efficiency

We calculated the internal quantum efficiency (IQE) by liquid Helium cooling system. We set 20K as IQE 100% point and compared to room temperature. We found the IQE for H_3PO_4 , KOH and reference sample is 15.7% , 3.7% and 13.4%, respectively. Fig 5.4.1 shows the IQE results. The H_3PO_4 has been improved, but the KOH sample decreased. The KOH sample may have some epitaxial problem in quantum well.

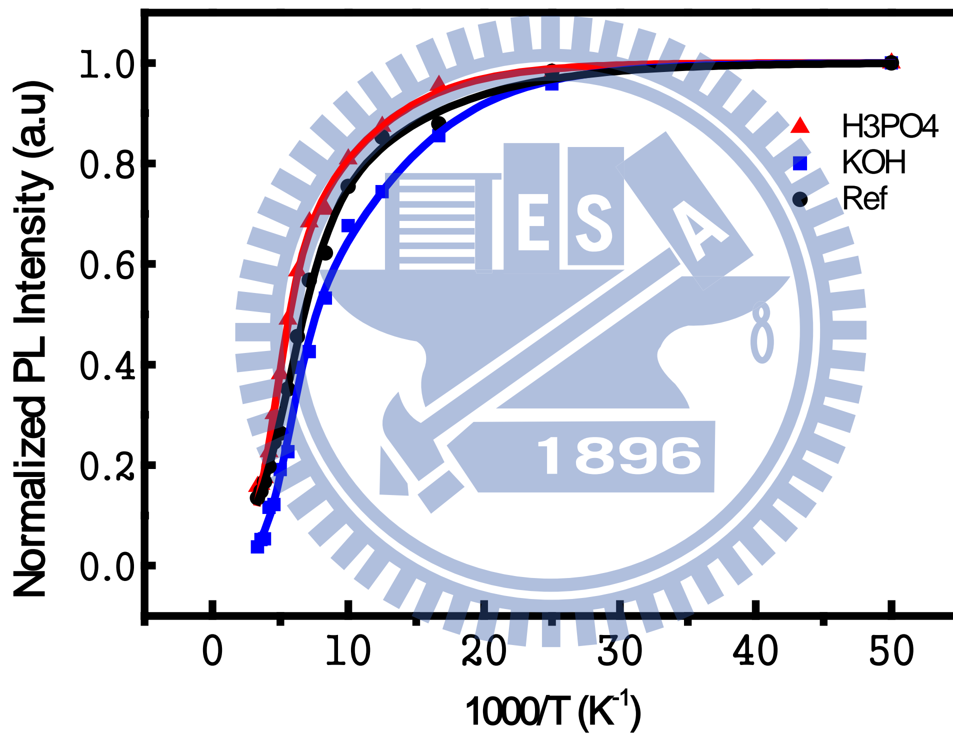

Fig. 5.4.1 The IQE results of LEDs

5.5 Reflection analysis

Fig. 5.5.1 shows the reflection of all LEDs. The reflection of H_3PO_4 and KOH sample are 2.6% and 2.1% higher than reference in wavelength 361nm. We verified the possibility that using silica nanopheres act as reflector in ultraviolet LED.

Fig. 5.5.2 shows the absorption of all LEDs. The absorption of H_3PO_4, KOH, and reference is 60%, 63%, 66%, respectively.

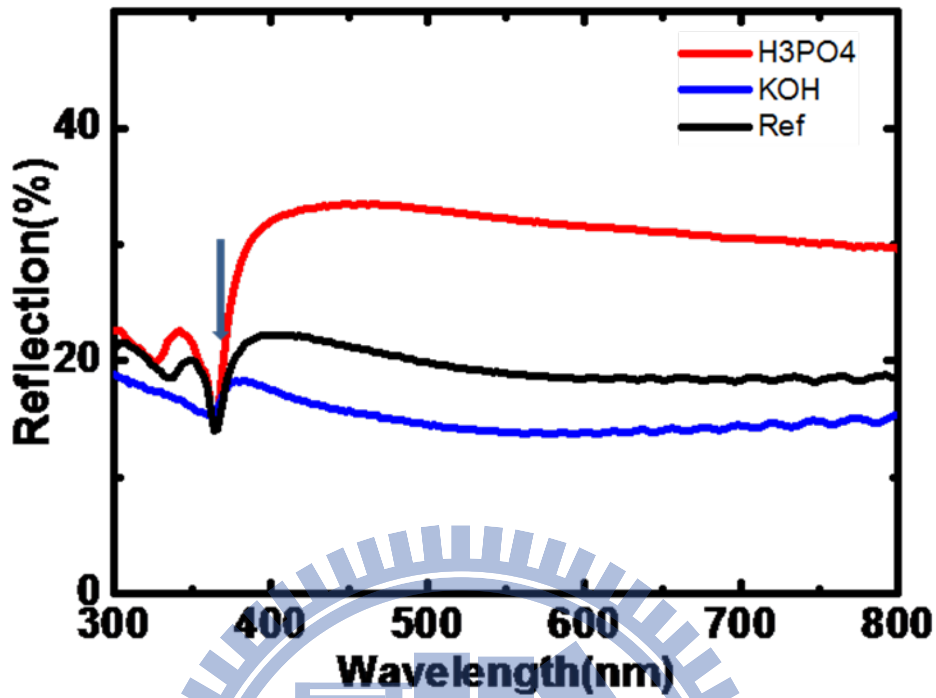

Fig. 5.5.1 Reflection of silica nanospheres embedded LED

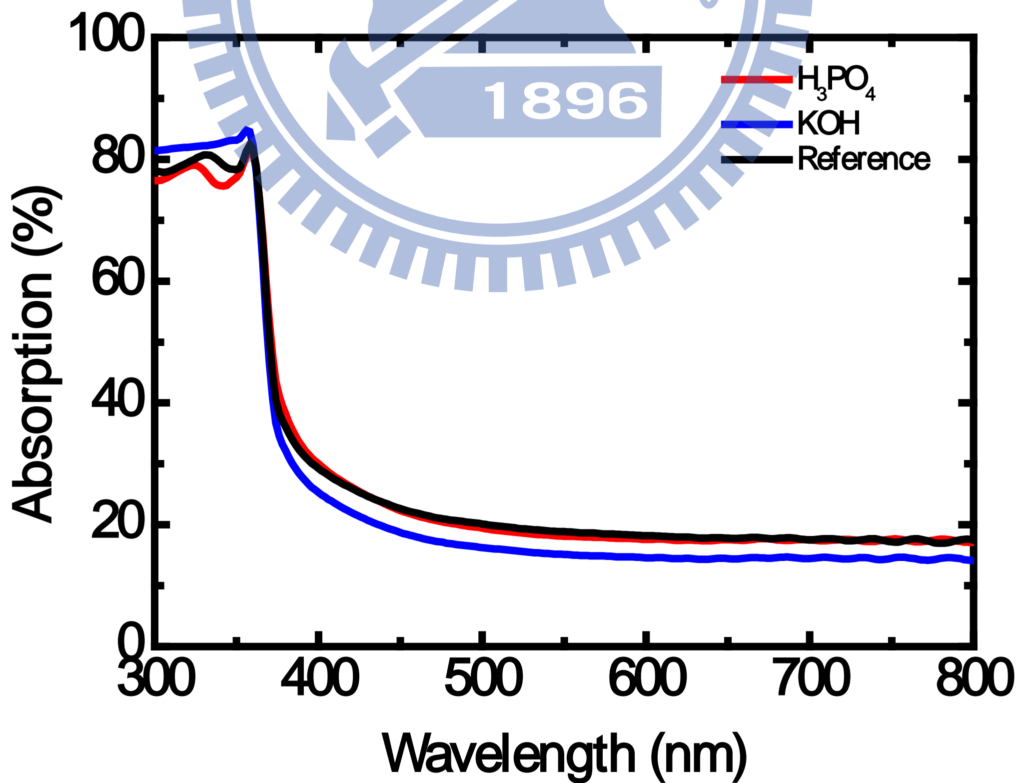

Fig. 5.5.2 Absorption of silica nanospheres embedded LED

Chapter 6 Conclusion

We simplified the defect passivation process (DSP), replacing PECVD and CMP process by embedding silica nanospheres. The DSP using silica nanospheres blocking the quantum well penetration of threading dislocation is much cheaper and convenience.

Furthermore, we confirmed that the H_3PO_4 prefer to etch screw type dislocation, which is treated as non-radiative centers. On the other hand, KOH prefer to attack edge type dislocation, which is considered no relation with non-radiative center.

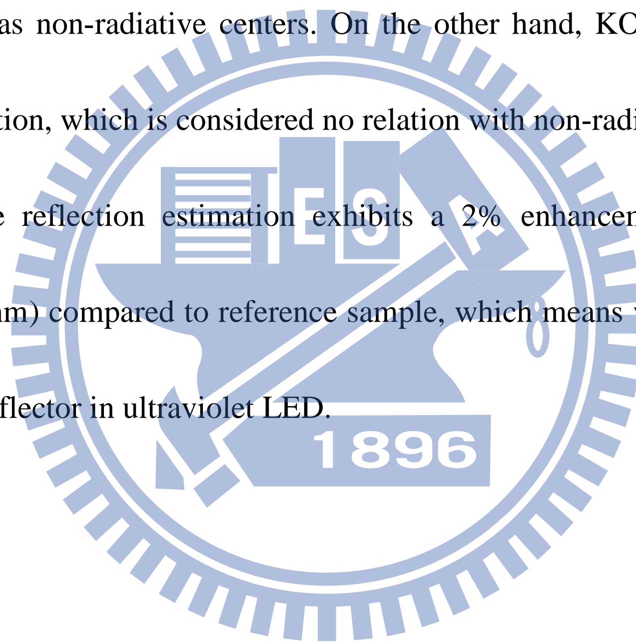

ES
1896

Finally, the reflection estimation exhibits a 2% enhancement in ultraviolet wavelength (361nm) compared to reference sample, which means we could use silica nanospheres as reflector in ultraviolet LED.